Journal of Marine Research, 52, 583–638, 1994

Circulation, transport and bottom boundary layers of the deep currents in the Brazil Basin

by X. Durrieu De Madron[1,2] and G. Weatherly[1]

ABSTRACT

Zonal and meridional hydrographic sections obtained for the South Atlantic Ventilation Experiment are used to study the circulation patterns and estimate the transports of North Atlantic Deep Water (NADW) and Antarctic Bottom Water (AABW) in the Brazil Basin.

The NADW Deep Western Boundary Current (DWBC) appears to be a relatively large ($\approx$800 km wide by 2 km thick), double core current, separated by counterflowing recirculation. It appears to split, branching seaward at the Cape Saõ Roque near 5S and again at the Columbia-Trinidad Seamount Chain at 21S. As a result of this latter bifurcation, the NADW DWBC flow in the southern basin decreases significantly.

In the southern part of the basin, the AABW DWBC is a relatively broad ($\approx$1000 km), thin ($\approx$700 m) flow which hugs the bottom of the continental rise. The densest waters that compose the core of the AABW DWBC eventually separate from the DWBC in the northern part of basin as they are topographically diverted to the east. The southward return flow at the eastern edge of the AABW DWBC and a northward flow in the eastern part of the basin suggest a meandering meridional recirculation of AABW in the interior of the basin. In the north central part of the deep basin there is a cyclonic abyssal gyre with a large component of Weddell Sea Deep Water (WSDW).

The along-isobath movement of the DWBCs over the sloping bottom drives cross-slope advection of the bottom boundary layer. The up-slope advection of denser water within the NADW DWBC is believed to set up a slippery bottom layer, while the bottom layer associated with the down-slope advection of lighter water within the AABW DWBC is estimated to be only partially slippery.

Geostrophic transports of heat, salt and mass are used to estimate mixing in the AABW flow in the Brazil Basin. The rates at which heat and salt mix are characteristic of diapycnal turbulent mixing. The mixing processes appear to be more active along the western boundary.

1. Introduction

The authors are involved in the observational component of the Deep Basin Experiment (DBE) of the World Ocean Circulation Experiment (WOCE). The DBE has two objectives: (1) to observe and quantify the deep circulation within an abyssal ocean basin, and (2) to understand how passages affect the flow of water through

1. Department of Oceanography, Florida State University, Tallahassee, Florida, 32306-3048, U.S.A.
2. Present addess: Laboratoire de Sedimentologie et Géochimie Marines, University of Perpignan, Avenue de Villeneuve, 66860 Perpignan Cedex, France.

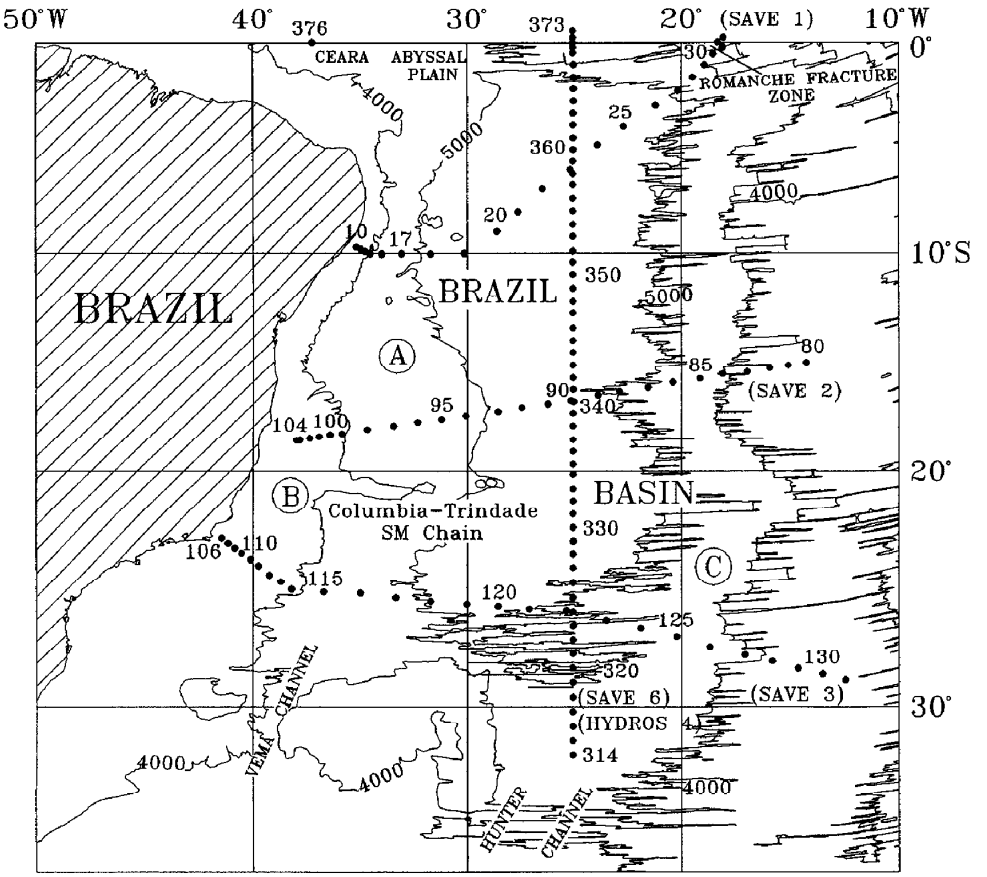

Figure 1. Bathymetry of the Brazil Basin and CTD station locations in this basin occupied during the SAVE1, 2, 3 and 6 legs. A-C denote boxes where budget estimates are later made in the text.

them (Hogg, 1990). The Brazil Basin (Fig. 1) has been chosen as the site for the DBE. The observational program, begun in 1992, is scheduled to terminate in 1995. Our contribution is to make moored current-meter observations of the deep western boundary currents (DWBCs) of North Atlantic Deep Water (NADW) and Antarctic Bottom Water (AABW) beginning in September, 1993. A mid-basin section, nominally along 18S, was selected.

After receiving notification of funding for the study we decided to examine the South Atlantic Ventilation Experiment (SAVE) data (described later) found in the atlas ATLAST (Rhines, 1991). The SAVE data set is one of the best data sets available for the Brazil Basin, and we wanted to determine from it whether we should modify the design of our moored current-meter array and/or relocate our section. While the vertical resolution of this data in ATLAST is coarse (values every 100 m to

300 m for depths $\gtrsim$ 1000 m), we found that the dynamic calculations and transport estimates made from it appeared reasonable. When the SAVE data set with finer, 2 db, vertical resolution became available through the National Oceanographic Data Center (NODC), we decided to repeat our analysis using the NODC SAVE data to see whether we would obtain essentially the same results. (We did.)

The present study describes the results of our examination of the circulation of NADW and AABW, particularly their DWBCs, in the Brazil Basin using the NODC obtained SAVE data. This study focuses on (1) the description of the vertical and horizontal structure, circulation patterns, and transport of the NADW and AABW DWBCs, (2) the sensitivity to the choice of level of no motion (LNM), (3) the abyssal mixing processes, (4) the downstream evolution of the bottom mixed layers in the DWBCs, and (5) the interior circulation. This paper is complementary to Tsuchiya *et al.* (1994) who collected and examined the water mass distribution and interior circulation along one of the SAVE sections examined here.

2. Review of the AABW and NADW circulation in the Brazil Basin

a. Physical setting

The Brazil Basin stretches from the equator to the subtropics ($\approx$30S) (Fig. 1). The deep part of the basin (>3000 m) is confined on the east and the north by the Mid-Atlantic Ridge, by the Brazil continental slope to the west, and by the Rio Grande Rise to the south. Although not indicated on the chart for reason of clarity, the northern part of the Brazil Basin is referred to as the Pernambuco Abyssal Plain and represents its deepest region. The major connecting passages between the Argentine Basin and the Brazil Basin are situated on both sides of the central elevation of the Rio Grande Rise: the Santos Plateau and the Vema Channel on the west and the Hunter Channel on the east. At the equator, the western trough between the Brazil Basin and the Guiana Basin is delimited by the zonally-oriented Mid-Atlantic Ridge and the continental margin of Brazil. The Romanche Fracture Zone represents the principle passage linking the Brazil Basin to the Guinea Basin on the eastern side of the Mid-Atlantic Ridge.

b. Hydrographic background

The characteristics of the waters in the western South Atlantic were reviewed by Reid *et al.* (1977). In the Brazil Basin, three major water masses are found beneath the permanent thermocline: the relatively cool, fresh and oxygen-poor Antarctic Intermediate Water (AAIW) formed in the Southern Ocean, the warm, salty, well-oxygenated NADW derived from the North Atlantic and the Arctic seas, and the colder, fresher, oxygen-poorer AABW formed around Antarctica. NADW is subdivided into three components (Wüst, 1935), the upper component (UNADW) derived from the Mediterranean Overflow Water, the middle (MNADW) associated

with the Labrador Sea Water and a lower component (LNADW) that originated in the Denmark Strait Overflow Water. In accordance with their densities, NADW is sandwiched between the overlying AAIW and the underlying AABW. Another water mass contributing to the vertical structure is the Circumpolar Deep Water (CDW). It is cooler and lower in salinity and oxygen than the NADW. This water mass, which is derived from Pacific waters entering the South Atlantic through the Drake passage, extends north with a density range encompassing that of the NADW. The meeting of these two water masses in the southern Brazil Basin causes a branching of the CDW into two layers above and below the NADW. The upper branch (upper CDW) is sandwiched between the AAIW and NADW layers. The lower branch (lower CDW), along with the abyssal layer of colder and less saline Weddell Sea Deep Water (WSDW), form the AABW.

c. Inflow of NADW

The southward flow of NADW in the North Atlantic is traced as a narrow, swift, western boundary current. Its circulation patterns in the western tropical North Atlantic and its penetration into the South Atlantic have been investigated fairly extensively in the last decade (e.g., McCartney, 1993 and the references therein). McCartney (1994) showed a consensus emerging from these recent studies, namely the existence of (1) a low latitude NADW DWBC transport on the order of 25.0–34.0 Sv (1 Sv = 10^6 m^3 s^{-1}), (2) a recirculation gyre over the Demerara Abyssal Plain north of the equator with a northward transport about 17.0 Sv and (3) a net southward NADW transport of about 17.0 Sv approaching the equator.

Several studies appraised the contribution of the different components of NADW north of the equator. Near 10N, Speer and McCartney (1991) estimated a southward transport between 1200 m (reference level) and 4400 m of 25.0 Sv. The contribution of LNADW, defined as between the depths of 2900 m and 4400 m, was about 10.0 Sv. Between 2N and 14.5N, Molinari *et al.* (1992) estimated the average southward transport below a reference level at 4.7°C at 25.9 Sv. They subdivided the transport above 1.8°C into three potential temperature classes, which yielded a contribution of the upper (3.2–4.7°C), middle (2.4–3.2°C) and lower (1.8–2.4°C) components of NADW of 4.4, 6.3, and 13.0 Sv respectively.

d. NADW flow in the Brazil Basin

While hydrographic (Wüst, 1935; Weiss *et al.*, 1989; Tsuchiya *et al.*, 1992, 1994) and direct current observations (Ponte *et al.*, 1990) support the existence of an eastward flow of UNADW along the equator, the major part of the NADW core crosses the equator to the south following the general trend of the Brazil continental slope (Defant, 1941; McCartney, 1993). At 11S, McCartney (1993) calculated a net southward transport of 12.9 Sv in the basin between 4°C (σ_2 = 36.7 kg m^{-3}) and 1.9°C, with a reference level along the 1.9°C isotherm. Near the western boundary,

the southward transport associated with the DWBC is about three times ($\approx$34 Sv) the net southward transport in the basin. Furthermore, there is a strong northward circulation, transporting 22.2 Sv, immediately off-shore of the DWBC. This northward flow is associated with a bowl-shaped density depression which is seen on several hydrographic sections across the Brazil Basin slope. McCartney (1993) suggested that this feature indicates an anticyclonic abyssal gyre along the western boundary of the Brazil Basin similar to the Demerara Gyre north of the equator.

Defant (1941), Reid (1989) and Zhang and Hogg (1992) described a broad recirculation of the NADW flow in the interior of the basin. They depict a southward NADW flow along the western boundary which deflects to the east south of 20S, flows to the north in the interior of the Basin and, finally turns to the northeast around 10S. Defant (1941) and Zhang and Hogg (1992) also show that one part of the NADW DWBC entering the Brazil Basin in the northwest separates from the southward flow of the DWBC around 5S. It, along with the recirculating water returning from the deep southern excursion, flows southeastward across the deep basin and then northeastward toward the equatorial region. This eastward flow of NADW in the Basin interior was also inferred by Tsuchiya *et al.* (1994).

e. Inflow of AABW

Below 2°C, temperature, salinity and oxygen decrease sharply. This isotherm is generally taken to be the boundary between the NADW and the AABW (Wright, 1970).

Warren and Speer (1991) showed the absence of any significant inflow of AABW north of the Walvis Ridge, on the eastern side of the Mid-Atlantic Ridge. This result emphasized the importance of the western basins as primary pathways for the equatorward flow of AABW. The principle passages from the Argentine Basin to the Brazil Basin are the Vema Channel, the Santos Plateau and the Hunter Channel. In the Vema Channel, Hogg *et al.* (1982) on the basis of current meter measurements estimated a transport of water denser than $\sigma_4 = 45.87$ kg m^{-3} at 4.05 $\pm$ 1.24 Sv, and at 4.15 $\pm$ 1.27 Sv on the basis of hydrographic data (reference velocity along the $\sigma_4 = 45.91$ kg m^{-3} isopycnal). More recently, Speer and Zenk (1993) estimated the northward flow below the 2.0°C reference level at 3.9 Sv. Likewise, they estimated the northward residual flow across the Santos Plateau between the Vema Channel trough and the western boundary to be 2.0 Sv, and the transport through the Hunter Channel on the eastern side of the Rio Grande Ridge to be 0.7 Sv. These estimates indicate that the AABW flow through the Vema Channel is about 4.0 Sv, and that the total AABW flow entering the Brazil Basin is about 7.0 Sv. Furthermore, Speer and Zenk (1993) suggest that the contribution of the WSDW (which they defined as water denser than $\sigma_4 = 46.05$ kg m^{-3}) to that inflow is about 40% ($\approx$2.7 Sv). The coldest waters observed in the Vema Channel are about -0.18°C (Hogg *et al.*, 1982;

Speer and Zenk, 1993), whereas those observed in the Hunter Channel are about 0.16°C (Speer and Zenk, 1993).

f. Flow of AABW in the Brazil Basin

There have been several geostrophic net transport estimates made along sections crossing the Brazil Basin at various latitudes. Using the IGY data, Wright (1970) estimated transports below a reference level of 1.9°C of 6.4 ± 1.6, 2.3 ± 0.6 and 2.8 ± 0.7 Sv at 24S, 16S and 8S respectively. From 1983 CTD surveys located at 23S and 11S, McCartney and Curry (1993) estimated transports below a reference level of 1.9°C of 6.7 and 5.5 Sv respectively. Similar estimates at 24S, 19S and 11S (Meteor 15 and Oceanus 133 sections), with a reference level along the σ_4 = 45.85 kg m^{-3} isopycnal, yield transports of 5.0 ± 1.1, 4.5 ± 0.8 and 3.0 ± 1.4 Sv respectively (Speer and Zenk, 1993). Apart from Wright's early estimate at 16S, these results show some recurrent trends in that: (1) the net northward AABW transport through the southern part of the Brazil Basin is about 5.0–7.0 Sv and, (2) there is a progressive basin-wide decrease of the equatorward net flow to the north.

In addition to the AABW moving as a DWBC in the western basin, Speer and Zenk (1993) inferred a weak, southward flow in the basin interior and a weak, northward flow in the eastern basin.

g. Outflow of AABW

AABW exits the Brazil Basin to the north across the equator and to the east through the Romanche Fracture Zone. McCartney and Curry (1993) estimate a trans-equatorial transport to the Guiana basin of 4.3 Sv. Northward spreading of AABW in the western basin of the North Atlantic Ocean at 4N was estimated by Whitehead and Worthington (1982) at about 2.0 Sv. However, their value may be too small; McCartney (1994) re-estimated it at 4.0 Sv. Thus, the transport estimates of McCartney (1994) and McCartney and Curry (1993) indicate an outflow of AABW across the northwestern channel of about 4.0 Sv. According to maps of properties distribution in the Ceara Abyssal Plain near 37W (McCartney, 1994), the minimum (bottom-most) potential temperature found at the equator is about 0.65°C ($\sigma_4 \approx$ 46.0 kg m^{-3}). This minimum increases farther north; at the latitude of the Ceara Rise ($\approx$ 4N) the coldest potential temperature is about 1.0°C. On the northeastern side of the basin, Warren and Speer (1991) inferred a transport of water into the Angola Basin from the Romanche Fracture Zone of about 2.0 Sv. Speer and Zenk (1993) reported that the waters flowing through the Romanche and Chain Fracture Zones are as cold as 0.8°C.

h. Mixing between AABW and NADW

At the same time as their transport estimates in the Vema Channel and the equatorial channel, Hogg *et al.* (1982) and Whitehead and Worthington (1982)

estimated the abyssal upwelling velocities and vertical diffusivities of heat and salt. Assuming that there is no exit for AABW below 1.0°C in the Brazil Basin, Hogg *et al.* (1982) estimated an upward advection rate across the 0.8°C and 1.6°C isotherms of 7.3 and 5.7 10^{-7} m s^{-1} (23 and 18 m y^{-1}) respectively. The downward heat flux required to balance the upward heat advection yielded a thermal diffusivity rate of 3–4 10^{-4} m^2 s^{-1} for the Brazil Basin. More recently, Speer and Zenk (1993) calculated an upwelling velocity (upward velocity across the 45.85 isopycnal) between 30S and 11S in the Brazil Basin of 8.0 10^{-7} m s^{-1}. Likewise, Whitehead and Worthington (1982) estimated cross-isotherm diffusion rates of heat and salt between 1°C and 1.9°C to about 1–4 10^{-4} m^2 s^{-1}. McDougall and Whitehead (1984) extended the study of Whitehead and Worthington (1982) to estimate the relative importance of isopycnal and diapycnal (across-isopycnal) mixing processes affecting the northward-flowing core of AABW north of the equator. Their study showed the predominant effect to be diapycnal turbulent mixing. While yielding results consistent with Hogg *et al.* (1982) and Speer and Zenk (1993), the results of Whitehead and Worthington (1982) perhaps need to be re-evaluated in light of McCartney (1994).

i. Bottom mixed layers over sloping bottoms

Classical and turbulent Ekman layer dynamics show that an arbitrary geostrophic flow above a flat bottom leads to a transport component normal to the geostrophic flow in the bottom layer. Recent studies indicate that the Ekman transport for flows oriented along isobaths over an inclined bottom in a stratified fluid can lead to profound effects on the dynamics of the flow (e.g., MacCready and Rhines, 1993, and the references therein).

The process is illustrated in Figure 2 for both a southward and northward flowing DWBC in the southern hemisphere. Advection in the bottom Ekman layer brings denser water upslope for a southward flowing DWBC and lighter water downslope for a northward flowing DWBC. This results in the bottom mixed layer (BML) for the southward flowing current being denser than if the BML formed over a level bottom. Conversely, this results in the BML for a northward flowing current being lighter than if the layer formed over a level bottom. The amount the BML is too dense or too light is indicated in Figure 2 by $\Delta\rho$. An important aspect is that the cross-slope advection sets up a buoyancy force that grows until it becomes comparable to the driving pressure gradient.

MacCready and Rhines (1993) point out that the resulting thermal-wind shear acts in both cases to reduce the velocity in the bottom layer. This, rather than friction, can be sufficient to bring the velocity to zero at the bottom. This reduction in velocity ΔV is given by:

$$\Delta V = \left| \frac{\alpha g}{f} \frac{\Delta\rho}{\rho} \right| \tag{1}$$

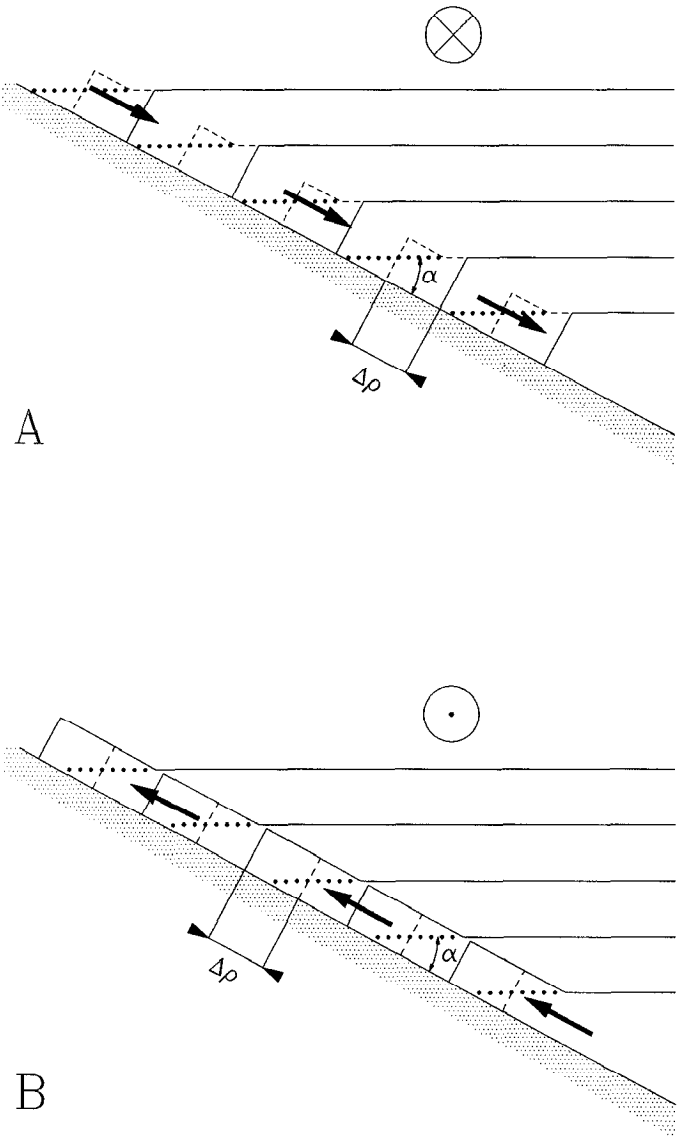

Figure 2. Schematic showing how Ekman transport in bottom boundary layers (arrow) over inclined bottoms can advect denser water upslope (upwelling) and lighter fluid downslope (downwelling). Solid lines are isopycnals, the dotted open circle represents interior flow out of the figure and the crossed open circle represents interior flow into the figure. The dashed lines denote level-bottom bottom layers, and the dotted line is the extrapolated interior profile. $\Delta\rho$ indicates the density anomaly in the bottom layer resulting from the across-slope advection of water. Ekman transport directions are for the southern hemisphere.

(ibid.) where α is the bottom slope relative to the isopycnal slope, g is the gravity, ρ is the density, f is the Coriolis parameter and $\Delta\rho$ is the density anomaly in the bottom layer resulting from the across-slope advection. Thus, after sufficient cross-slope Ekman advection has occurred, the bottom layer of a DWBC may be frictionless.

The time τ_0 for the BML to become slippery is about

$$\tau_0 = C|f|/(\alpha N)^2 \tag{2}$$

where N is the buoyancy frequency in the interior, and

$$C = 2 \text{ for upwelling,}$$

$$10 \text{ for downwelling}$$

(ibid.). The reason for C's value depending on whether upwelling or downwelling is occurring is due to the asymmetric response of the bottom layer to upwelling and downwelling. A downwelling layer's thickness is greater than that of a level-bottom layer while an upwelling layer's thickness is about equal to that of a level-bottom layer (Weatherly and Martin, 1978). In addition, the downwelling layer's BML thickens with time due to advection, while the upwelling layer's BML thins with time due to the thickening, by diffusion, of the density jump which caps it (MacCready and Rhines, 1993; this density jump is seen in Fig. 2B). Finally, the thermal wind reduction ΔV in (1) occurs across the BML of a downwelling layer while in an upwelling layer it occurs across the density jump capping the BML.

Taking for the NADW DWBC $N = 1.7 \times 10^{-3}, f = -0.5 \times 10^{-4}\ s^{-1}$, $\alpha = 0.01$, and $C = 2$ gives $\tau_0 \approx 4$ days. Taking for the AABW DWBC $N = 1.5 \times 10^{-3}\ s^{-1}, f = -0.5 \times 10^{-4}\ s^{-1}$, $\alpha = 0.002$, and $C = 10$ gives $\tau_0 \approx 650$ days. The times τ_0 should be compared to transit times of the DWBCs from their entrances into the Brazil Basin. For example, with DWBC speeds of about 5 cm s^{-1} the transit time to the SAVE2 section (close to the basin's mid-latitude) for both DWBCs is about 400 days. The τ_0 for the NADW DWBC suggests that its bottom layer is slippery and is too dense. Garrett *et al.* (1993) conclude that a slippery bottom layer is no longer turbulent, and consequently that it restratifies due to vertical diffusion. MacCready and Rhines (1993) note that the same diffusion process should cause a slippery layer to thicken slowly downstream. This further suggests that the bottom layer of the NADW DWBC is stratified with little evidence of a BML, and it slowly thickens downstream. For a restratified upwelled bottom layer $\Delta\rho$ is the density anomaly across the bottom layer relative to that for a bottom layer formed over a level bottom. The τ_0 for the AABW DWBC suggests that its bottom layer is only partially slippery, that it is too light, and that it has a BML which thickens downstream (due to downslope advection of lighter water rather than vertical diffusion).

3. Data and analysis techniques

a. Hydrographic data

The hydrographic data examined here are the SAVE observations from the Brazil Basin which we obtained from the NODC. The northernmost section (SAVE1) was made between November 23 and December 13, 1987. It crosses the northeastern part of the Brazil Basin obliquely, but is zonal along 10S in the western part (Fig. 1). The mid-basin section (SAVE2) was made between December 18, 1987 and January 23, 1988. It crosses the Brazil basin at between 15 and 19S (Fig. 1). The southernmost section (SAVE3) was completed between January 29 and March 7, 1988. It crosses the western part of the Brazil basin between 23°40′S and 28°40′S (Fig. 1). The meridional section (SAVE6 or HYDROS4) was made between March 13 and April 19, 1989 along the 25W from 32S to 0°40′N.

The NODC data consist of vertical profiles of conductivity, temperature, pressure and dissolved oxygen from the surface to within ≈ 10 m of the bottom in 2 dbar increments. All density values (σ_0, σ_2, σ_4 referred to 0, 2000 and 4000 dbar respectively) quoted in this paper are calculated according to the International Equation of State (EOS80). All the salinity values are on the Practical Salinity Scale (PSS78). The Brunt-Väisälä (buoyancy) frequency was calculated using the adiabatic leveling method as described in Fofonoff (1985).

The 2 dbar data were smoothed with a gaussian filter with a half-width of 10 dbar. The 10 dbar smoothed data were mapped by linear interpolation. In order to preserve the continuity of the hydrographic structures along the sloping bottom, the interpolation procedure was performed on a density grid (σ_4) and then interpolated back on the depth grid.

b. Geostrophic calculations

Relative geostrophic velocities were computed using the dynamic method (the thermal wind relation). Absolute geostrophic velocities were then inferred by assuming a LNM between AABW and NADW. However, a problem arises along a sloping bottom when the deepest common level (DCL) lies above the LNM. A usual solution then is to assume a zero velocity at the DCL; this is equivalent to assuming a zero near-bottom velocity. However, another solution is available for the Brazil Basin. The LNM can then be raised to be between NADW and AAIW. It will be shown in Section 4 that these two methods give similar but not identical results.

For some steep bottom slopes near the western boundary, station spacing did not adequately resolve the bottom topography. Relatively small-scale features of the density distribution near the sloping bottom have a large effect on the geostrophic transport. However, the transport estimate in the bottom triangle between two adjacent stations of different depth is derived from vertical extrapolation of the velocity profile down to the deepest station depth. The extrapolation method used here follows that described by McCartney (1994). It extrapolates the velocity linearly

at a point below the DCL by using the vertical velocity shear above the DCL weighted by the ratio of the vertical density gradient at the point below the DCL to that above the DCL. The weighting procedure uses the vertical density profile of the deeper station. This extrapolation method implies, for example, a constant velocity in the bottom mixed layer when it is located below the DCL. The transport derived from this method is higher (by a maximum of 50%) than that derived by considering a constant velocity through the bottom triangle.

The geostrophic relation degenerates as the equator is approached, because the Coriolis force goes to zero there. We terminate the velocity and transport estimates for the SAVE1 and SAVE6 sections at a few degrees south of the equator ($\approx$ 3S).

4. Distribution of properties: review and results

The distribution of properties along the meridional section SAVE6 or HYDROS4 has been thoroughly analyzed by Tsuchiya *et al.* (1994). They also considered the HYDROS3 section which together with the SAVE6 section forms a continuous quasi-meridional section spanning the entire western South Atlantic (from 54S to the equator).

Our work was done independently of theirs. Our conclusions about the distribution of NADW and AABW along the SAVE6 section are very similar to theirs. Thus, the comments made in this section about the distribution of properties of these water masses along the meridional section should be considered as a review of results already presented in Tsuchiya *et al.* (1994) unless otherwise stated. Similarly, the θ, S, σ, and O_2 meridional sections shown here should also be considered as taken from Tsuchiya *et al.* (1994). They are presented here partially for the convenience of the reader, partially for completeness, and partially because they are integral to our determination of the flow patterns presented later.

The different water masses (NADW and AABW) are clearly revealed in the hydrographic sections (potential temperature, salinity, potential density anomalies, buoyancy frequency and oxygen) displayed in Figures 3 to 7 as well as in the θ-S diagram shown in Figure 8.

NADW. NADW is recognized as a warm, salty and oxygen-rich water spanning the depths from about 1200 m ($\sigma_2 \approx 36.70$ kg m^{-3} or $\theta \approx$ 3–4°C) to about 3500 m ($\sigma_4 \approx 45.87$ kg m^{-3} or $\theta \approx 2$°C) over the whole basin. The western boundary carries the strongest signal. The trace of NADW in the interior of the Brazil Basin is clearly visible along the meridional section at 25W. Its signal vanishes progressively south of 25S, where it is replaced by CDW of southern origin. Two cores are also evident, one in the equatorial region and the other in the southern part of the basin. The three components of NADW are easily distinguished in the northern core, while in the southern core NADW appears to be a more homogeneous mixture of these three waters.

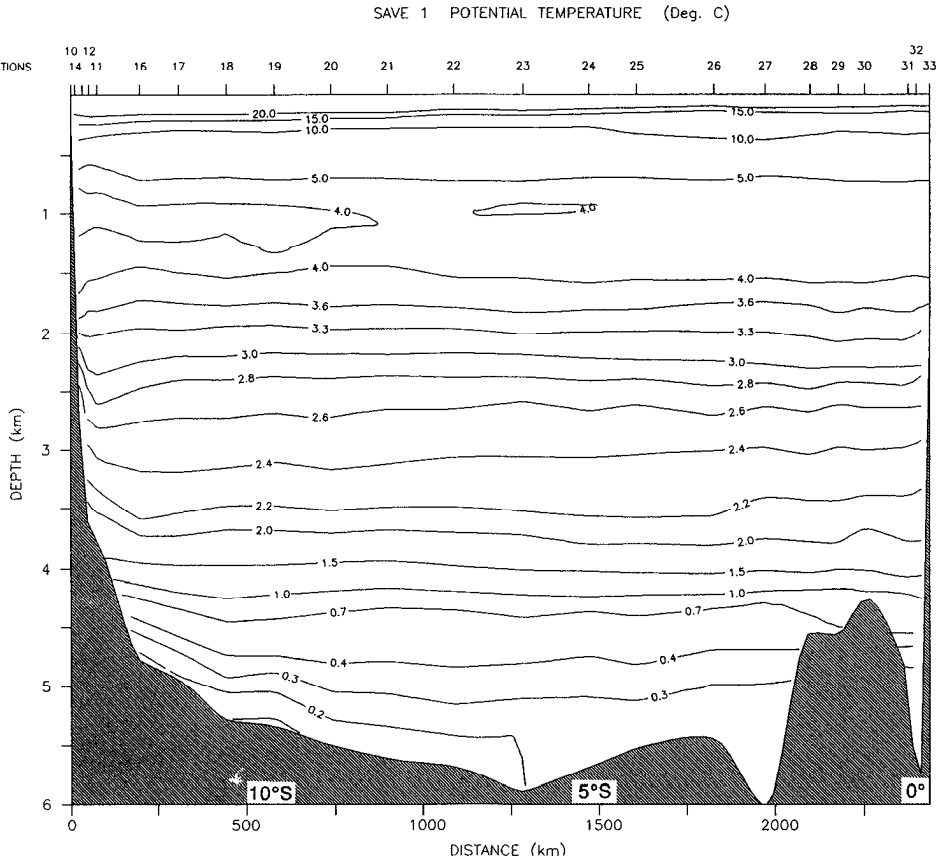

Figure 3. Profiles of potential temperature (°C) along the different sections: (A) SAVE1, (B) SAVE2, (C) SAVE3 and (D) SAVE6 (HYDROS4). Station numbers are along top, depth scale (km) along left side, and distance (km) from western or southern edge along bottom axis. Nominal longitude or latitude is shown at bottom.

The upper part of NADW (UNADW) extends at depths between about 1200 and 1900 m. In the southern part of the basin, NADW is progressively replaced by UCDW of southern origin, characterized by a slightly lower salinity and oxygen signature. It lies beneath the AAIW layer that is clearly defined as a low salinity tongue extending into the interior of the basin and along the western boundary at depth around 800 m (Fig. 4). UNADW is characterized by maximum temperature at about 1400 m (Fig. 3) and maximum salinity at about 1800 m depth (Fig. 4). The salinity maximum is clearly observed along the western boundary. It is also observed in the double core feature along the axis of the basin at 25W, one core north of 12S (with two maxima) and the other around 22S. The latter core is located eastward of the Columbia-Trinidad Seamount Chain which stands in the way of the southward-

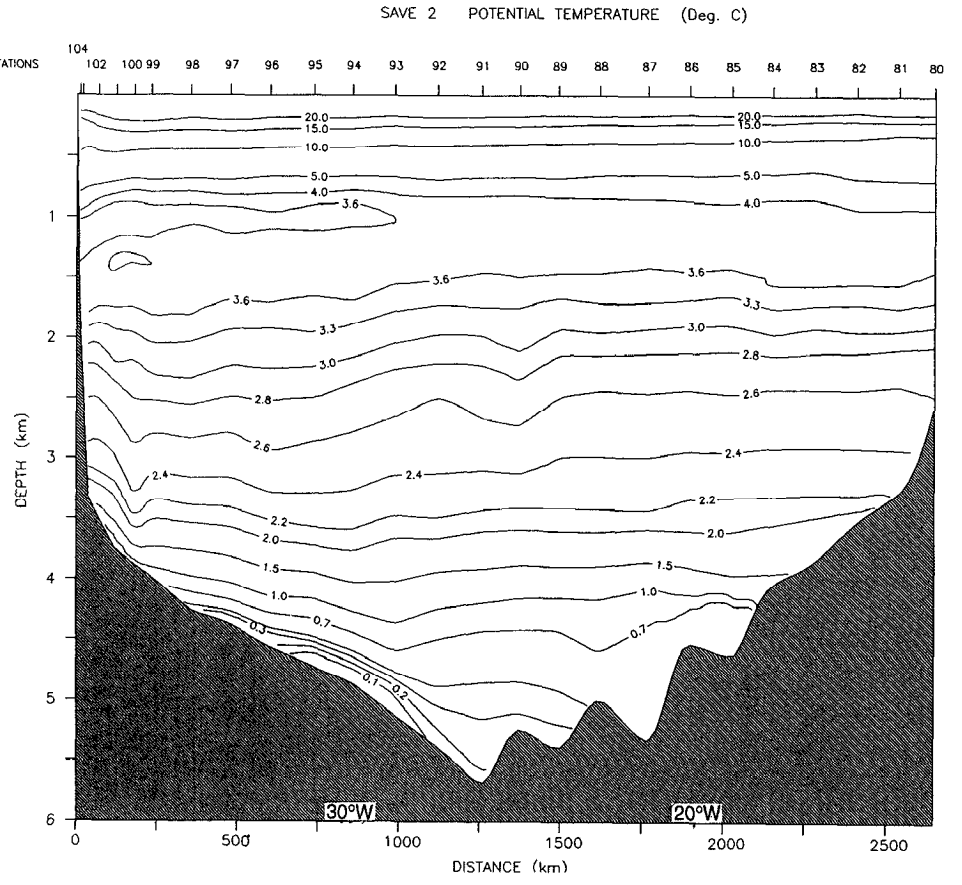

Figure 3. (Continued)

flowing DWBC, and indicates an eastward excursion or bifurcation of at least part of NADW DWBC.

The middle part of NADW (MNADW) is characterized by an oxygen maximum centered around 2000 m (Fig. 7). The σ_2 = 36.95 kg m^{-3} isopycnal ($\theta \approx 3.4$°C) is adopted as the surface delimiting UNADW and MNADW. Two MNADW oxygen maxima clearly appear in the Brazil Basin, one along the western boundary and the other in the interior of the basin north of 12S. Although decreasing in concentration, the westernmost oxygen maximum skirts the western boundary all along the basin. The northern oxygen maximum can be traced along the meridional section at 25W and along the northeasterly SAVE1 section. At 25W, this tongue of MNADW is separated in two cores, one extending southward from the equator down to 6S and the other centered around 10S. Farther south, another deep high salinity and high oxygen core appears along the axis of the basin as a core centered at about 22S.

Another deeper oxygen maximum is apparent at a depth of around 3500 m in much

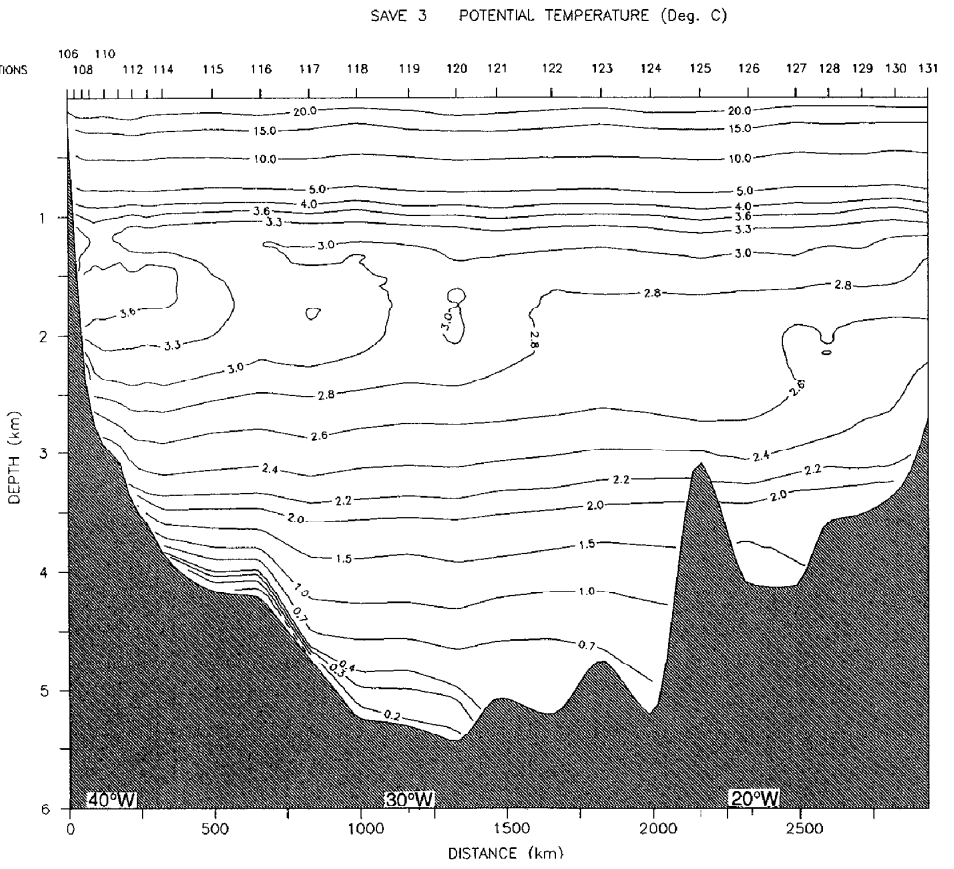

Figure 3. (Continued)

of the basin (Fig. 7). This deep oxygen maximum represents the lower part of the NADW (LNADW), and is separated from the MNADW by an oxygen minimum located along the $\sigma_2 \approx 37.02$ kg m^{-3} isopycnal. The core of LNADW generally coincides with a basin-wide minimum stability layer at a depth roughly between 2200 m and 3500 m (Fig. 6). In the northern basin, the layer of LNADW is nearly continuous, extending eastward from the western boundary at 10S to the equator along the SAVE1 track and southward from the equator to about 12S along the meridional section at 25W. South of the Columbia-Trinidad Seamount Chain, the high oxygen concentration cores shift from the western boundary to the interior of the basin (SAVE3 section). A trace of this eastward shifting of LNADW is also observed on the mid-basin section at 25W as part of the southernmost salinity and oxygen maximum.

A bowl-shaped density structure between 100–200 km in breadth (Fig. 5) is observed somewhere between 100 to 300 km offshore of the Brazil continental slope

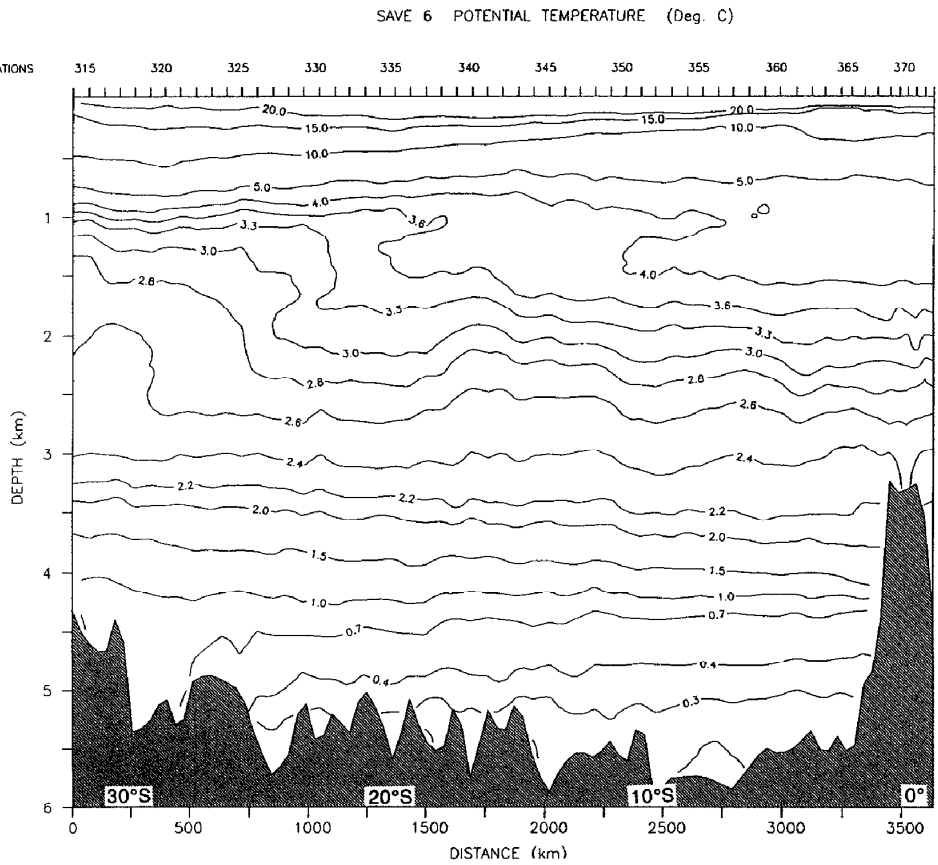

Figure 3. (Continued)

at a depth ranging between 2000 m and 4000 m. A similar feature is seen off the Brazil continental slope in Fuglister (1960) and McCartney (1993). This dipping of isopycnals is apparently a permanent feature. Its structure is best resolved at 19S, where it deepens down to the bottom. Its amplitude and vertical extension is smaller at 24S. At 10S, the density structure close to the slope is probably incompletely resolved due to the large distance and the great bottom-depth difference between stations 11 and 16. In particular, the density depression could be more pronounced between these two stations.

AABW. The strong vertical gradients of potential temperature, salinity and oxygen that appear below LNADW are generally taken to be the boundary between NADW and AABW. The 1.9–2.0°C isotherms are thus traditionally chosen as the top of AABW. However, Reid *et al.* (1977) identified the boundaries of the different water layers in the South Atlantic by strong vertical density shear (high static stability – or

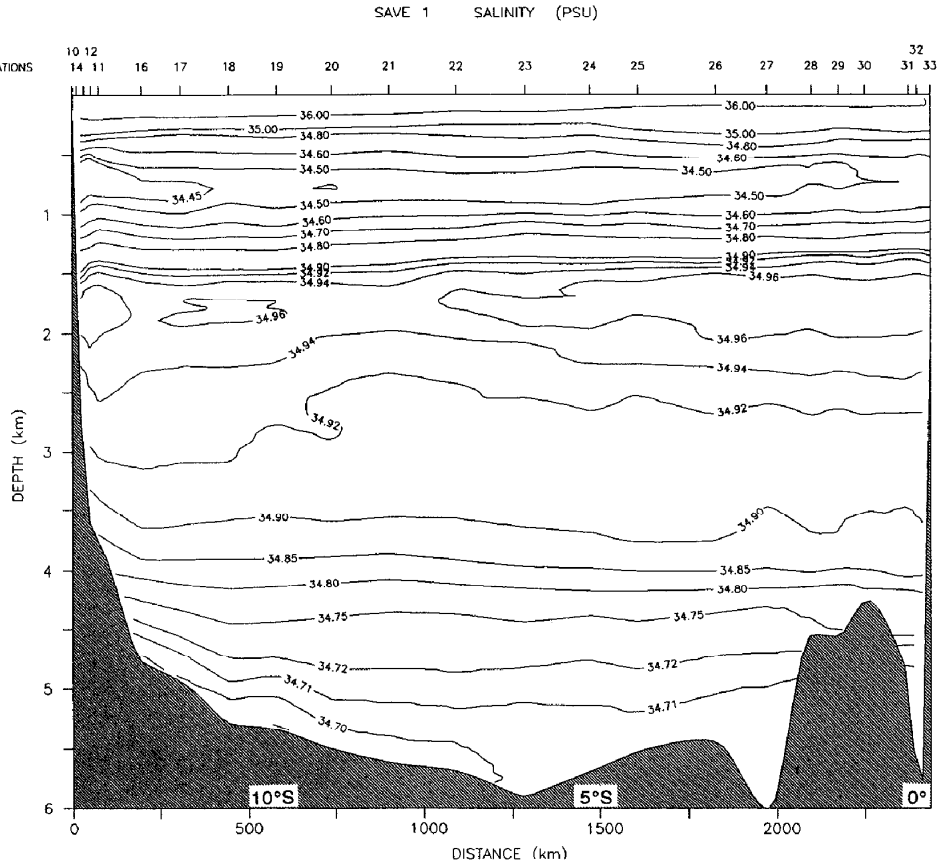

Figure 4. Same as Figure 3 but for salinity (psu).

buoyancy frequency) strata. A high stability stratum is observed all over the Brazil Basin (Fig. 6) along σ_4 = 45.90–45.95 kg m^{-3} ($\theta \approx 1.5$°C), and corresponds to the inflexion points of the temperature and salinity profiles. This suggests a boundary between NADW and AABW slightly deeper than the conventional 2°C isotherm ($\sigma_4 \approx$ 45.85–45.87).

Another and deeper high-stability stratum appears between the 46.01 and 46.04 isopycnals on the western side of the basin. This stratum is clearly observed at 24S and 19S but is no longer visible at 10S. The cold, low salinity tongue of water, denser than σ_4 = 46.0 kg m^{-3} extends as a strong feature along the axis of the basin, decreasing in thickness from the equator to about 25S. Less oxygenated waters, also the coldest, freshest and densest, along 25W, are found in the northern part of the Pernambuco Abyssal Plain. Speer and Zenk (1993) characterized the WSDW entering the Brazil Basin through the Vema channel by an increase in oxygen concentration near the bottom, and adopted the σ_4 = 46.05 kg m^{-3} isopycnal as the

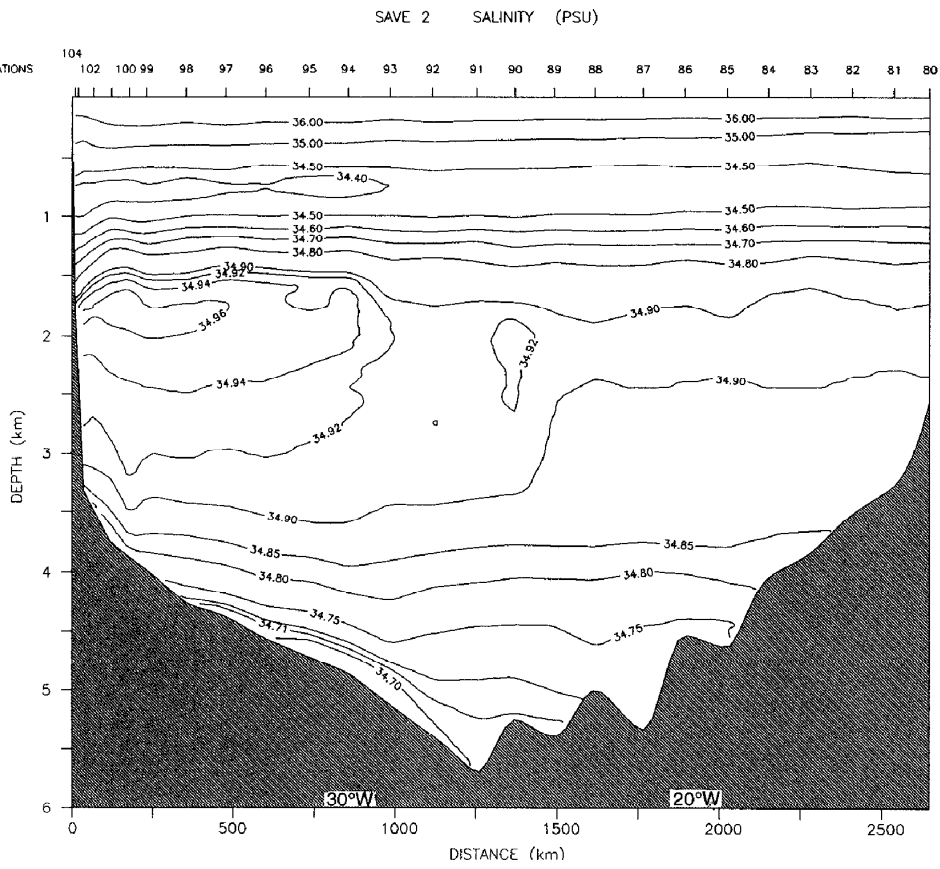

Figure 4. (Continued)

interface between the WSDW and LCDW. While this bottom increase in oxygen concentration is observed in the AABW DWBC at 24S, it is no longer visible farther north along the western boundary. The absence of a stratum of maximum stability between LCDW and WSDW at 10S suggests an homogenization of these two water types between 19S and 10S. However, part of the large body of dense water in the northern Pernambuco Abyssal Plain shows a minimum of oxygen around σ_4 = 46.04 kg m^{-3} (Fig. 7). The water column underneath this minimum is weakly stratified (Fig. 6) and is believed to indicate a storage of WSDW within the northern Pernambuco Abyssal Plain which apparently was not noted by Tsuchiya *et al.* (1994).

5. Results

a. Geostrophic velocity field

Reference level. Two reference levels are commonly considered along the western boundary of the Brazil Basin. A shallower reference level is sometimes chosen at the

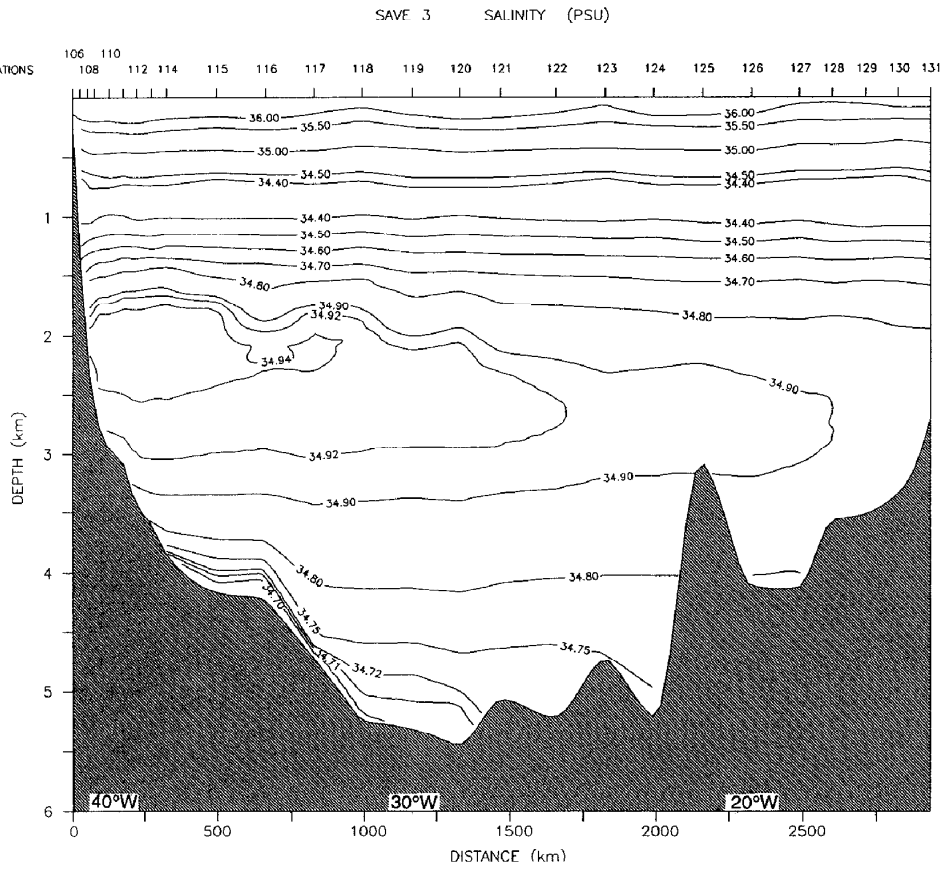

Figure 4. (Continued)

transition between the northward flow of AAIW and southward flow of UNADW (e.g., Speer and McCartney, 1991). As noted earlier, the transition layer between AAIW and NADW is taken along the $\sigma_2 = 36.7$ potential density surface. A deeper LNM is also supposed to separate the southward flow of NADW and northward flow of AABW. According to the vertical density gradient structure, the boundary between NADW and AABW is better defined by the $\sigma_4 = 45.90$ kg m^{-3} isopycnal. However, we choose the $\sigma_4 = 45.87$ kg m^{-3} isopycnal as the reference level to match the 1.9–2.0°C isotherms and to allow transport comparisons with previous studies.

We found that the different choices of reference level (deeper LNM and zero near-bottom velocity above it, upper LNM, combined deep and shallow LNMs) yield qualitatively similar velocity fields for the DWBCs (i.e., southward flow of NADW at mid-slope depth and a northward flow of AABW along the continental rise). However, some transport estimates for the NADW and AABW DWBCs show large differences depending on the choice of reference level. For example, the DWBC's

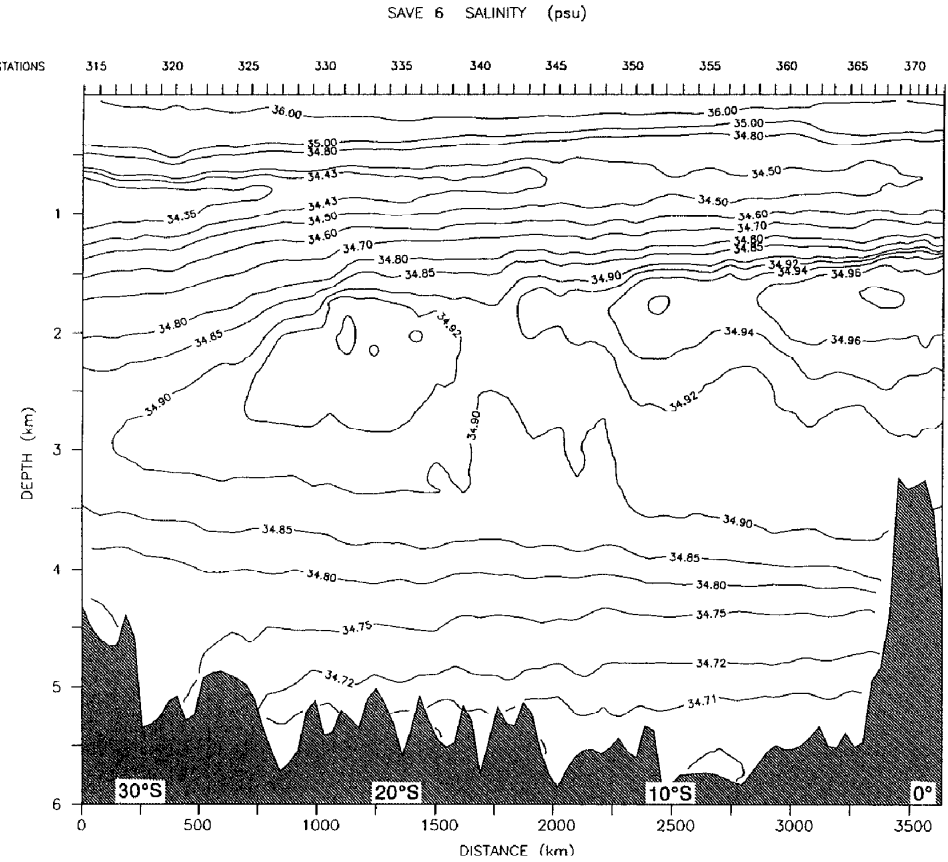

Figure 4. (Continued)

transport estimates with the upper LNM alone are more scattered from section to section than the transports calculated with the deeper LNM. The differences of the two estimates is up to ±60% for the NADW DWBC and about ±20% for the AABW DWBC. Therefore a reference level at the interface between AABW and NADW appears to be better suited to the SAVE data set, because it gives a more consistent picture and less scattered transport estimates of both NADW and AADW DWBCs. Furthermore, NADW transport estimates along the slope (where there is no AABW), using either a near-bottom zero velocity or a shallow LNM at the NADW/AAIW interface, yield similar results.

Note that the LNM between NADW and AABW is used over the entire basin. This was done for comparison with earlier studies (e.g., Wright, 1970; McCartney and Curry, 1993; Speer and Zenk, 1993). While this LNM probably does not apply throughout the basin, the resultant inferred flow field will later be seen to be consistent with many features of the property distribution in the basin interior.

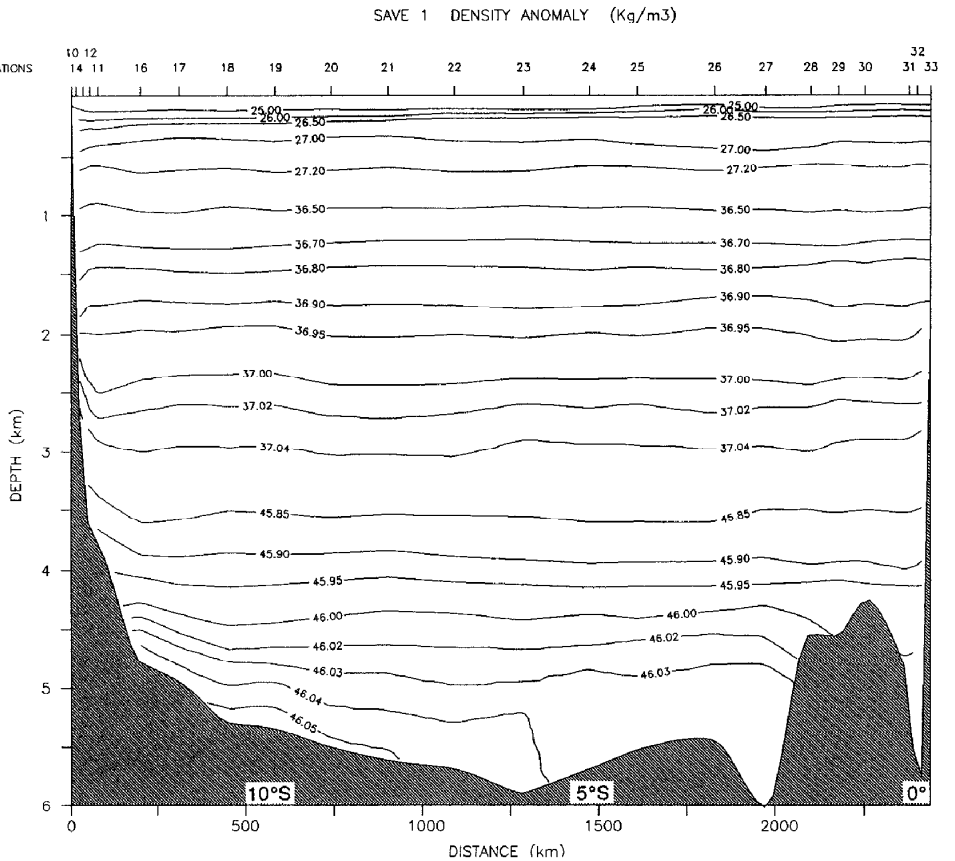

Figure 5. Same as Figure 3 but for potential density anomaly (kg m^{-3}) referenced to 0 dbar, 2000 dbar and 4000 dbar (1 dbar = 1 kPa).

Circulation along the western boundary. The contours of geostrophic velocity for the four sections are displayed in Figure 9. The most intense circulation is meridional and takes place near the western boundary.

In all sections intersecting the western boundary a double core feature appears within the main NADW high-salinity and oxygen-rich core that extends from the slope to roughly 800 km off-shore. Thus the NADW DWBC consists of two cores, relatively narrow (<300 km) and swift (up to 40 cm s^{-1} close to the slope), and separated by a region of counter (northerly) flow. This northward flow, located on the outer side of the isopycnal dip, is believed to characterize a recirculation of deep water within the southward-flowing NADW DWBC.

The northward flowing AABW DWBC appears as a 1000 km wide vein of variable thickness that hugs the rise between roughly 3500 and 5000 m depth. At about 24S and 19S, the vein of the DWBC coincides with the densest core of AABW (Fig. 5). The velocity increases down to the bottom, where it attains a maximum of about

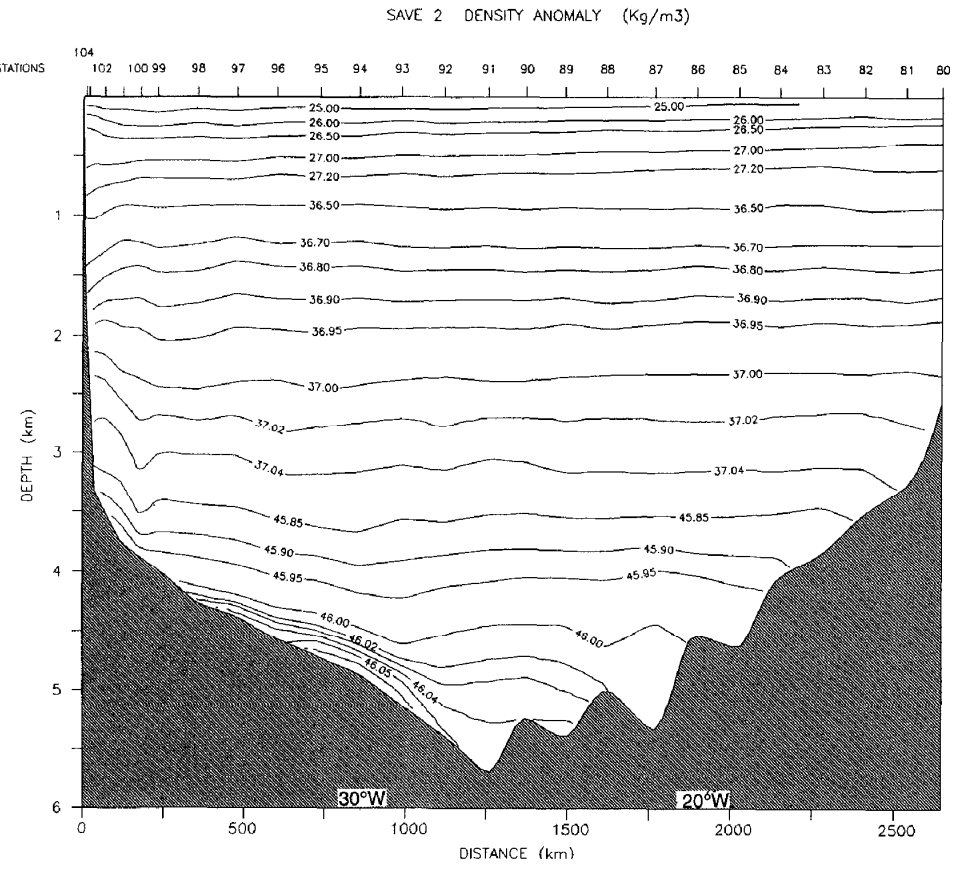

Figure 5. (Continued)

4 cm s^{-1}. At 10S, the DWBC vein is narrower ($\approx$ 500 km) and shifted westward of the densest core of AABW. It exhibits maximum (extrapolated) bottom velocity as high as 10 cm s^{-1}.

Circulation in the interior of the basin. The velocity sections are contaminated by bands of alternating flows which in the zonal sections are linked to the station spacing. This small-scale noise in the flow field masks the basic features of the flow field in the interior of the basin, where the velocities are weak. A 2nd order Butterworth spatial filter was used to remove the high wave-number signal (Pickart and Smethie, 1993). The half response amplitude of the low-pass filter corresponds to a 350 km wave length. The filtering of velocities was done along density surfaces. The resulting filtered velocity sections are shown in Figure 10.

Although this smoothing obliterates most of the internal structure of the NADW DWBCs, the gross features of the large-scale circulation in the basin are more

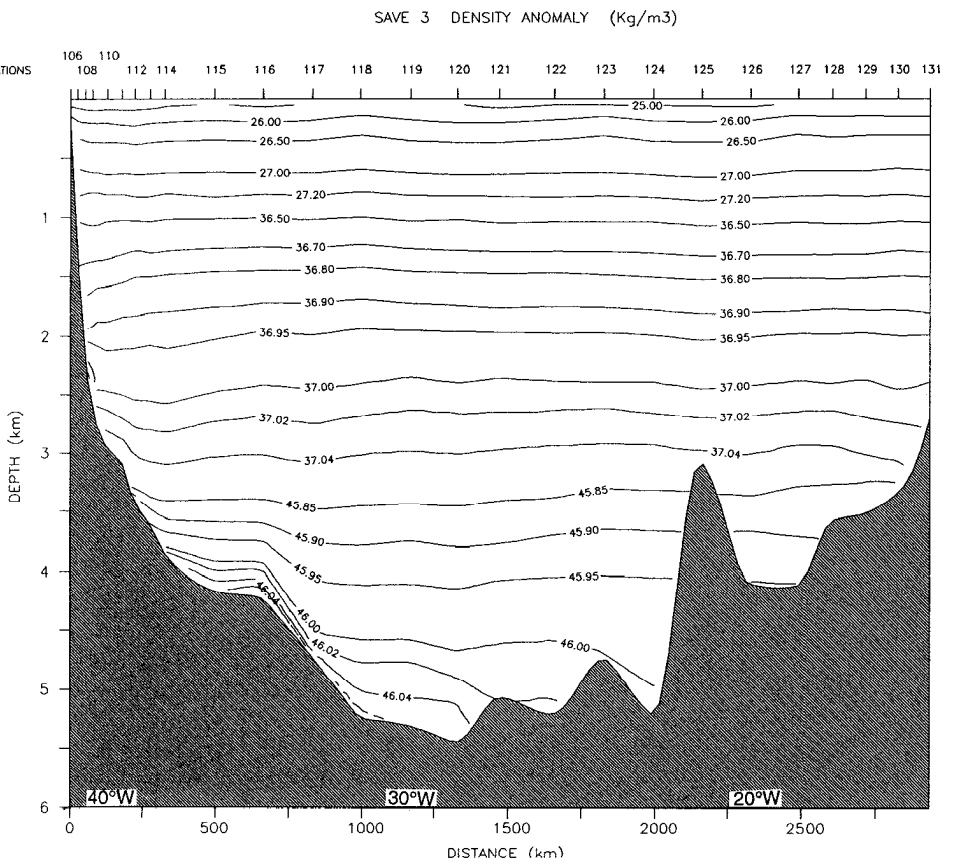

Figure 5. (Continued)

clearly revealed and are consistent with the distribution of properties. The NADW meridional circulation in the interior of the basin is weak (≤ 1 cm s^{-1}) and is dominated by a broad northward counterflow with a stronger core close to the DWBC. The zonal circulation along the axis of the basin shows a westward flow (mainly composed of CDW) south of 25S and an eastward flow of NADW between 25S and 15S. Together with the northward flow off-shore of the DWBC, these features indicate an anticyclonic recirculation in the interior of the basin. The northward flow of NADW in the interior of the basin is composed of water cooler, fresher and less oxygenated than that along the western boundary. This alteration of the NADW signal presumably results from mixing with CDW that circulates westward (and eventually northward) in the southern part of the basin. North of 15S, the layer around the oxygen minimum, roughly between 2500 m and 3000 m depth, is advected westward. Part of this westward flow of cooler, fresher, less-oxygenated waters is believed to join the outer branch of the southerly DWBC between the

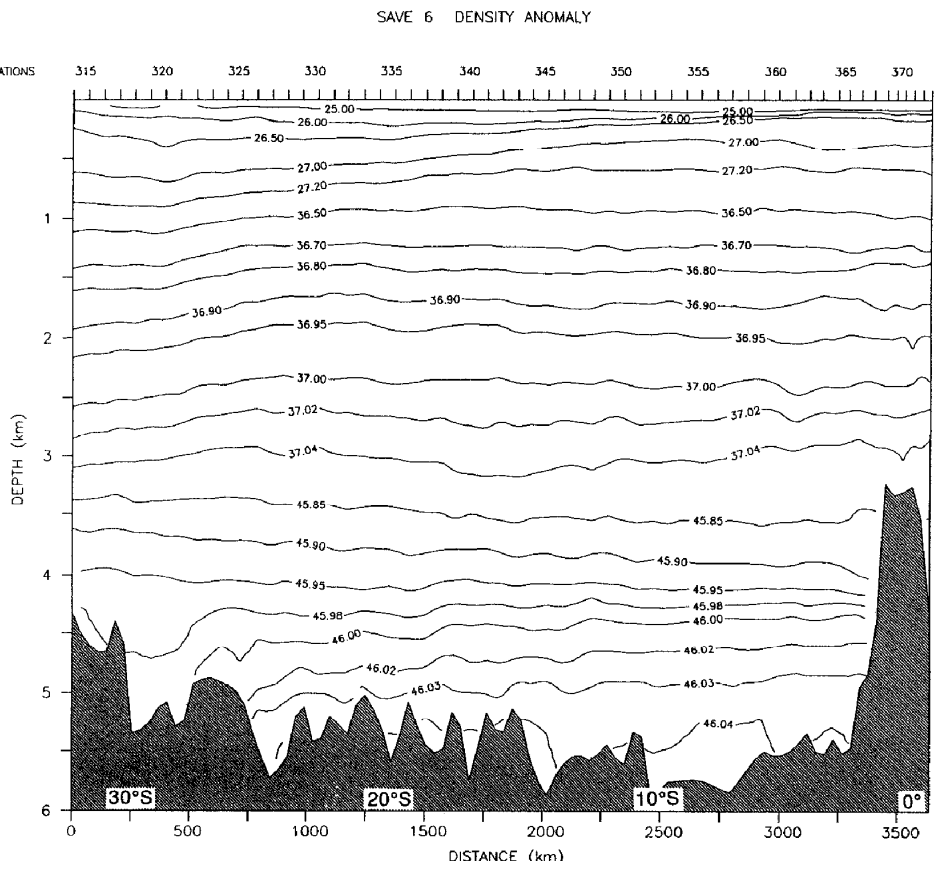

Figure 5. (Continued)

SAVE2 and the SAVE1 sections. The mixing of these two flows is likely to result in the increased thickness of minimum oxygen layer that separates the two oxygen maxima of MNADW and LNADW along the western boundary.

The circulation patterns along the meridional section north of 12S confirm flow patterns inferred by Tsuchiya *et al.* (1994). The upperlaying eastward flowing UNADW and MNADW (between roughly 1300 m and 2500 m depth) is separated into two cores by a counter flow centered around 8S. This double core feature coincides well with the distribution of properties, which shows two high-salinity and high-oxygen cores separated by a fresher and less-oxygenated water. These same features are also reproduced on the SAVE1 section at approximately the same latitudes which reinforce the conclusion of Tsuchiya *et al.* (1994) that the eastward flows result from a branching of the NADW DWBC near the equator.

The AABW DWBC appears clearly in contact with the bottom all along its width. The flow of bottom water denser than σ_4 = 46.01 kg m^{-3} lies too deep along the

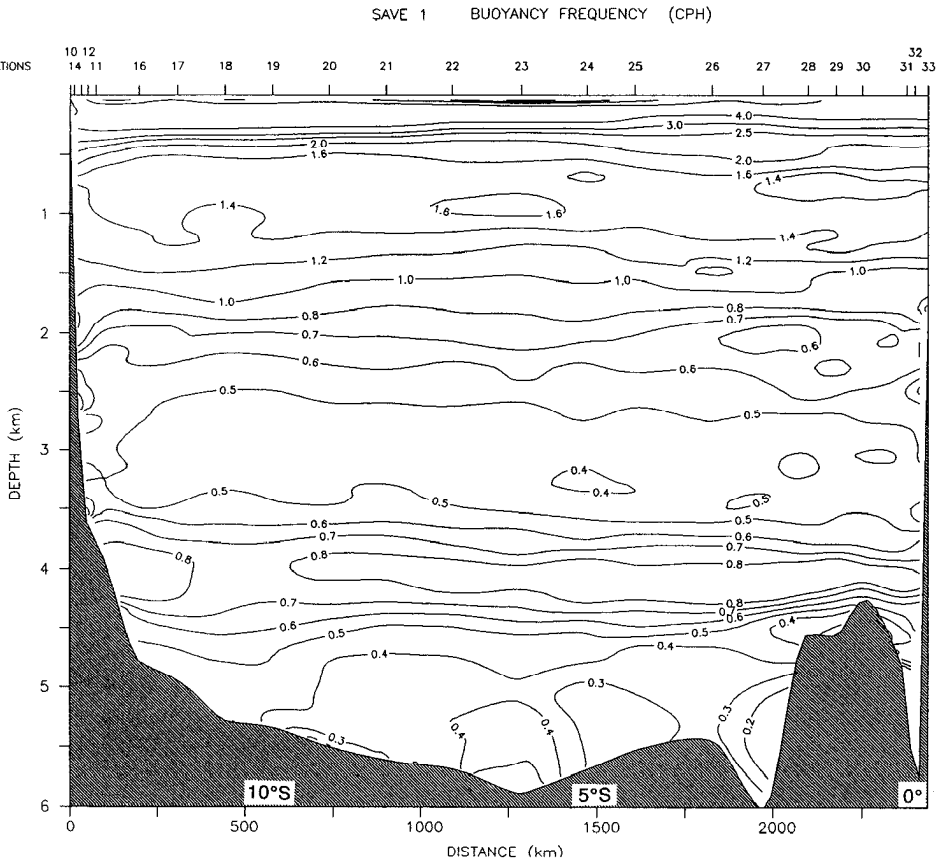

Figure 6. Same as Figure 3 but for buoyancy frequency (cph).

western boundary of the Brazil Basin to enter the Ceara Abyssal Plain directly, and is forced by the topography to turn east. The displacement of the AABW DWBC from the densest water at SAVE1 indicates that the easterly diversion of the densest water has begun to occur at 10S. Part of this dense water and the overlying water flows back toward the south. In the zonal sections, this return flow is seen at the eastern edge of the DWBC, carrying water slightly warmer and saltier than the DWBC. On the eastern flank of the basin, the currents are predominantly northward; this suggests that the return flow finally turns back to the Pernambuco Abyssal Plain, carrying increasingly warmer and saltier waters. The progressive warming and increasing salinity along the path of the AABW throughout the basin is clearly depicted in Figure 8B. The meridional mid-basin velocity section suggests a meandering of these abyssal flows across the axis of the basin. Some intense cyclonic circulation associated with the bulk of dense water in the northern part of the Pernambuco Abyssal Plain is indicated. The existence of this abyssal gyre is also supported by the presence of two

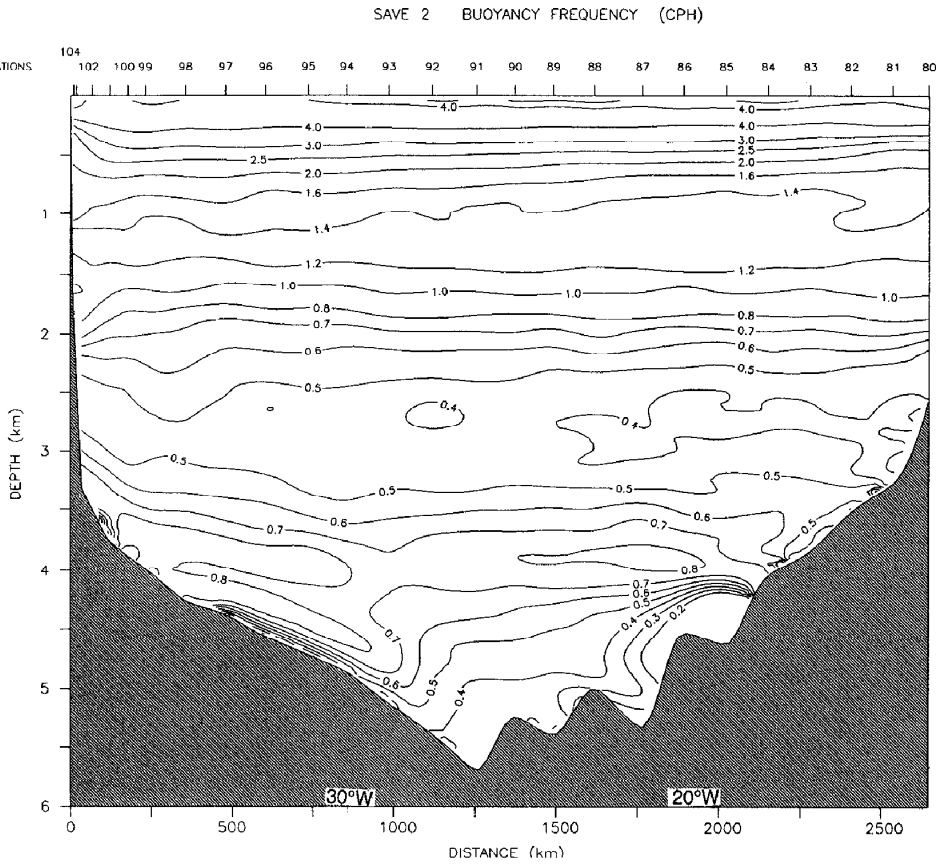

Figure 6. (Continued)

cores of minimum oxygen (at 9S and 4–5S in Figs. 7A,D) and weak density stratification (Figs. 6A,D) associated with each part of the gyre.

b. NADW and AABW transport estimates

Transports of NADW and AABW are estimated from the unfiltered geostrophic velocity field. All the transport estimates given here are vertically integrated between each station pair and within the density range delimiting the water mass layers. The density surfaces used to separate the different water mass layers are summarized in Table 1.[3] The results are displayed as graphs of cumulative transport integrated along the different sections (Figs. 11 and 12). The cumulative transports reproduce

3. Tsuchiya *et al.* (1994) gave a careful description of the evolution of the depth and density of the maxima of salinity (UNADW) and oxygen (MNADW and LNADW) along the 25W section. We chose mean density values for the interfaces between these water masses to simplify the calculations. In light of the uncertainty of the LNM in the basin interior, including variable bounding density surfaces does not seem warranted.

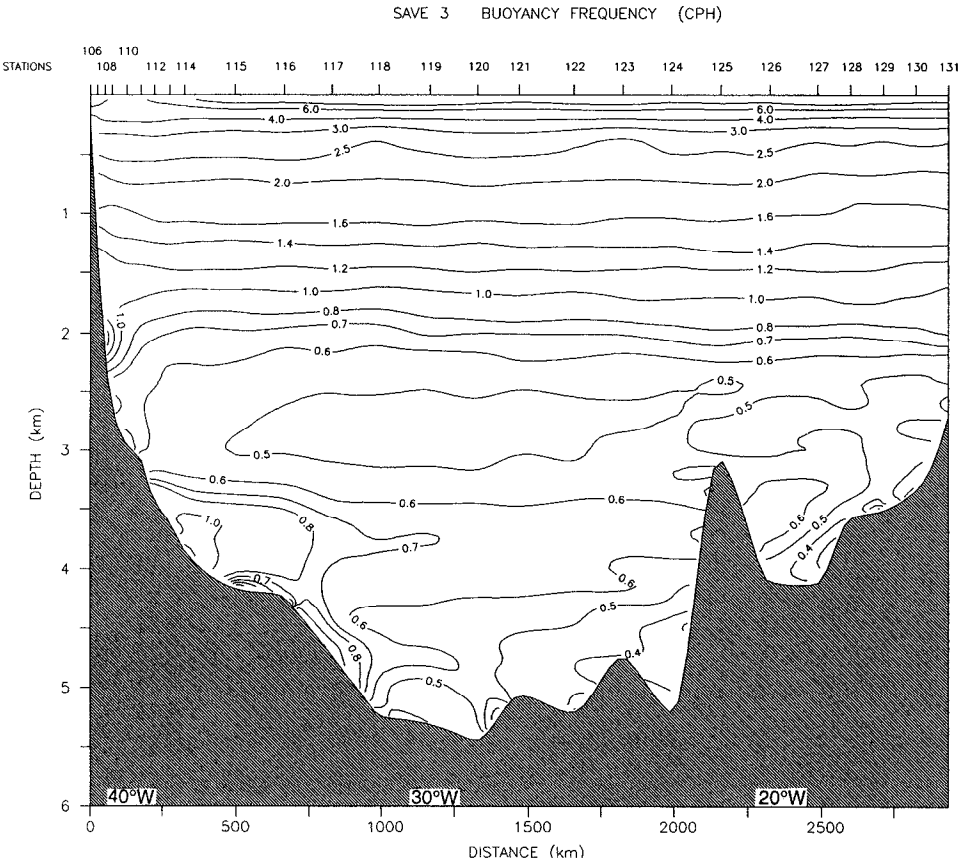

Figure 6. (Continued)

the trend of the flow field as inferred both from unfiltered velocity sections for the DWBC and the filtered velocity section for the interior circulation. It indicates that the noise in the velocity field affects the accumulated transport estimates only slightly.

NADW. Transport estimates of NADW and its components for the different sections are presented in Figure 11. The errors implied by moving the reference level by ± 0.03 kg m^{-3} ($\approx \pm 0.2$°C) amount to less than 25% for the transport estimates. The bottom triangle transport contributes to less than 7% of the transport along the slope. The transport in the closed boxes along the western boundary delimited by the sections shows an imbalance for the NADW layers with an overall convergence of 5.0 Sv in the northwestern box (box A, see Fig. 1) and of 10.0 Sv in the southwestern box (box B, see Fig. 1).

Cumulative transports evidence the two southward-flowing branches of the NADW

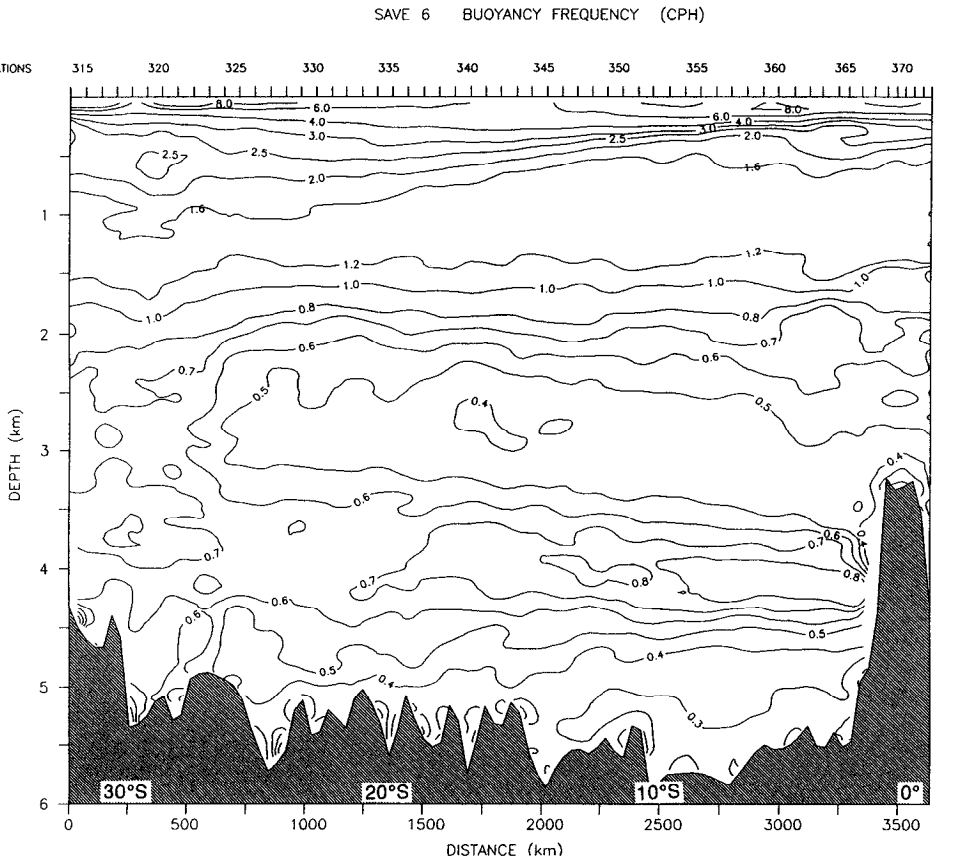

Figure 6. (Continued)

DWBC that are partly balanced by the northward recirculation between them. The southward transport of the inner NADW DWBC branch accounts for about two-thirds of the total southward DWBC transport (sum of the inner and outer branch transports). The total southward DWBC transport is estimated to 26.5 Sv at 10S and 24.4 Sv at 19S, then reduces to 7.1 Sv (9.2 Sv using the upper reference level along the slope) at 24S. The DWBC is larger in transport because of the recirculating component that transports about 5.6 Sv between 10S and 19S, and 4.4 Sv near 24S. Thus the net southward transport of the NADW DWBC (including the contributions of both inner and outer branches minus the northward recirculation) amounts to 20.8 Sv at 10S. This transport is essentially unchanged at 19S, where it is about 19.0 Sv. It reduces drastically to 2.7 Sv (4.9 Sv using the upper reference level along the slope) at 24S.

The inverse method of Hoffman and Worley (1986) was applied to box B along the southwestern boundary (see Fig. 1) in order to reduce the NADW unbalanced

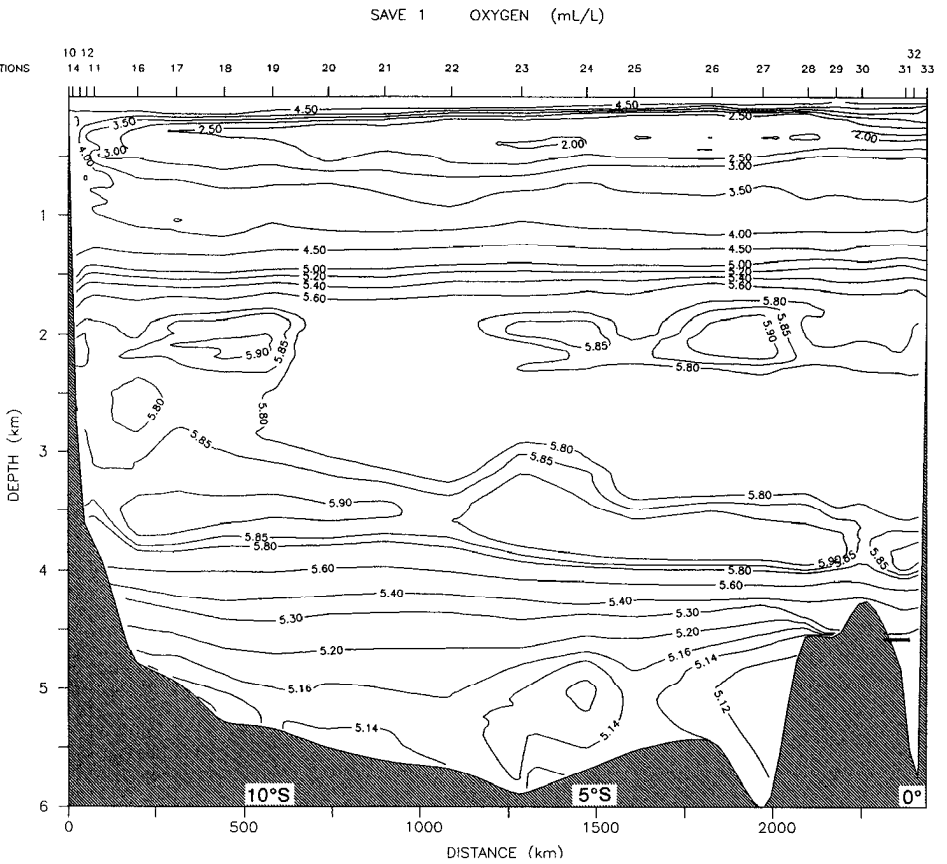

Figure 7. Same as Figure 3 but for dissolved oxygen concentration (ml l^{-1}).

transport in this box ($\approx$ 10 Sv). Considering relative geostrophic velocities calculated with an initial reference level along the σ_4 = 45.87 kg m^{-3} and a zero DCL velocity along the slope, the absolute geostrophic flow field was determined by imposing mass conservation constraints in the layers of AABW, the three components of NADW (Table 1) and the overlying upper layer. This linear least-squares problem considered an error tolerance of 1.5 Sv for each layer and inverse square root weighting (ibid.), and the inversion procedure used the singular value decomposition. In the interior the correction velocities were small, being of the order of 0.1 cm s^{-1}. Large corrections up to 8 cm s^{-1} were found along the slope for the SAVE3 section. While the southward transport of the NADW DWBC at 19S was unchanged, about 19.0 Sv, this inverse method yielded a larger transport at 24S, about 10.6 Sv. Although the estimates of the NADW DWBC transport at 24S are different and may not be considered as definitive, they all indicate a large reduction of the NADW DWBC between 19S and 24S. This decrease of the southward transport also exists across the

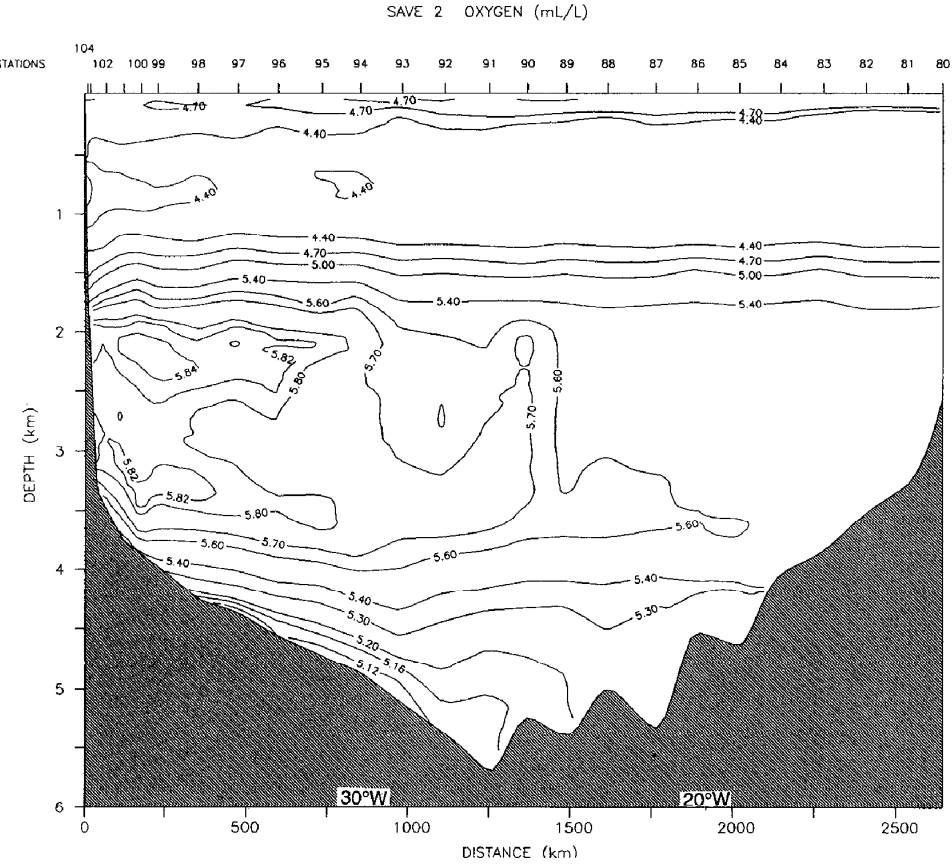

Figure 7. (Continued)

whole basin. The NADW transport along the SAVE1 section up to station 26 is about 11.0 Sv. It is about 12.0 Sv along the SAVE2 sections ($\approx$ 15–19S) and reduces to zero (or 9.0 Sv with the inverse calculation) along the SAVE3 sections ($\approx$ 24–29S).

A very narrow core of northward-flowing UNADW appears against the western boundary. This transport is probably associated with the northward flow of UCDW and AAIW along the slope. While it is nonexistent at 24S, it increases from about 1.6 Sv at 19S to 8.5 Sv at 10S.

The hydrographic structures reveal a bifurcation of the DWBC around the latitude of the Columbia-Trinidad Seamount Chain (a similar bifurcation is indicated in Wüst, 1935; Reid, 1989 and Tsuchiya *et al.*, 1994). The transport of the eastward component is estimated to be 7.8 Sv at 25W. In the interior and on the eastern boundary of the basin, the northward return flow of NADW/CDW is about 3.0 Sv at 25–28S and about 6.0 Sv at the basin's mid-latitude. The increase in transport of the northward interior flow between 25S and 18S emphasizes the confluence of the

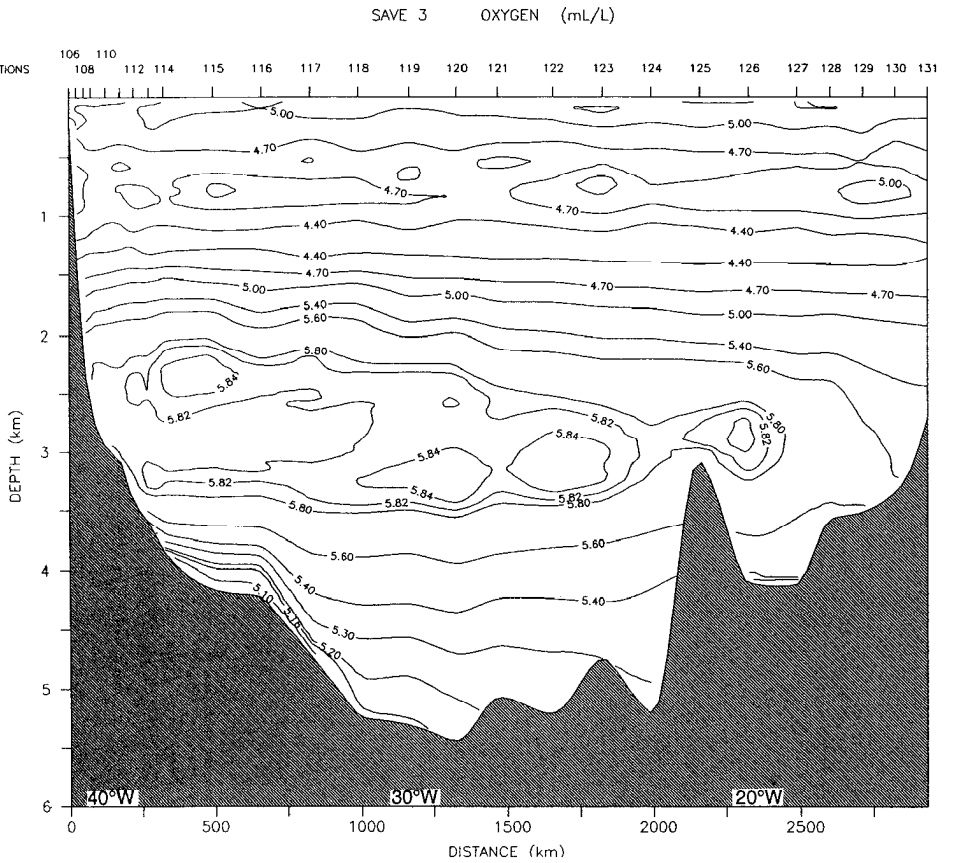

Figure 7. (Continued)

anticyclonic recirculation of NADW with some northward flow of CDW. As on the smoothed velocity section (Fig. 10), the major transport of this equatorward recirculation appears along the axis of the basin immediately offshore of the southward-flowing DWBC.

The westward flow of fresher and less oxygenated water between 15S and 12S transports 5.6 Sv (Fig. 11D). The eastward flow of NADW near 12S, estimated to be 4.9 Sv, is about two thirds of the transport of the outer branch of the DWBC at 10S (7.2 Sv). The rest (2.3 Sv), may be advected southward with the outer DWBC and may add to the 5.6 Sv from the westward-flowing branch of the recirculation. This would yield a transport of 7.9 Sv, which is close to the transport of the outer DWBC, estimated near 19S (8.0 Sv).

The west-northwestward return flow near 8S is visible for both the SAVE6 (previously inferred by Tsuchiya *et al.*, 1994) and SAVE1 sections and amounts to about 6.0–7.0 Sv. Only part of the northernmost eastward flow of NADW along the equator was estimated because of the degeneracy of the geostrophic equations near

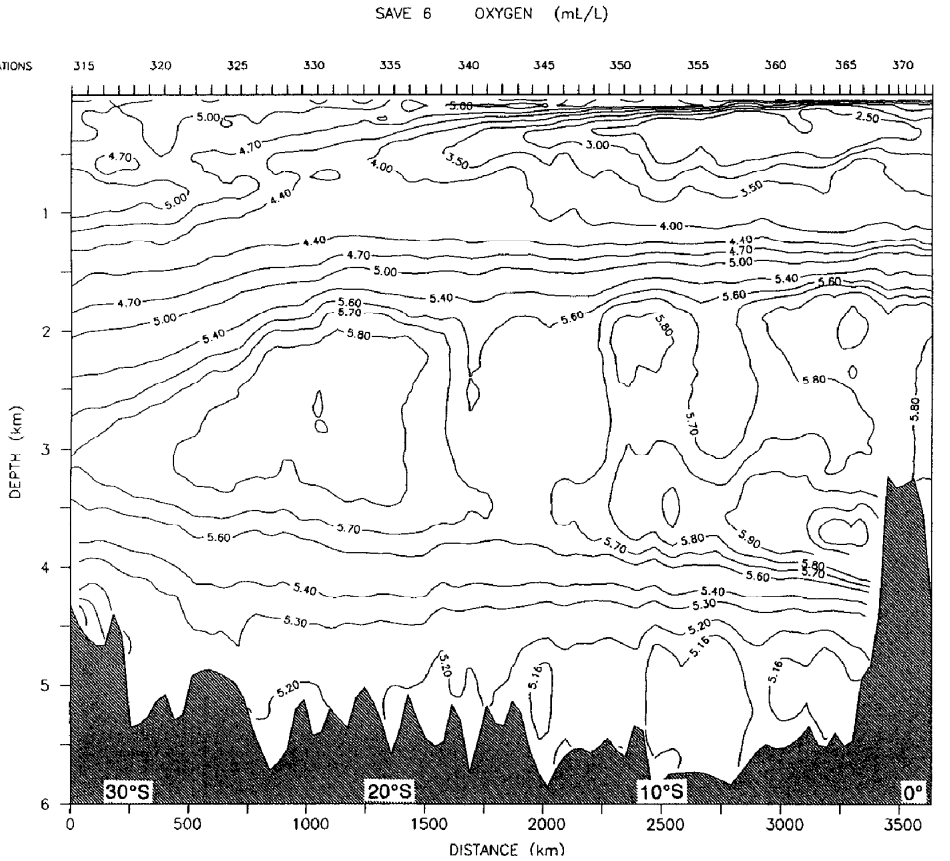

Figure 7. (Continued)

the equator. This eastward flow appears to be separated by a westward flow around 3S, and the transport of the branch south of this counter flow is about 6.0–10.0 Sv.

AABW. Transport estimates of AABW and the contribution of two density classes to this flow for the different sections are presented in Figure 12. The errors implied by moving the reference level by ± 0.03 kg m^{-3} (≈ ±0.2°C) amount to less than 20% for the transport estimates. The inverse calculation yields comparable but somewhat lower transport estimates (about 10–20%) of the AABW DWBC at 23S and 19S. The bottom triangle transport contributes to less than 30% of the transport for the SAVE2 section, but represents up to 50–60% of the AABW DWBC transport for the SAVE1 and SAVE3 sections. However the DWBC transport estimates along those two sections are less reliable because of the coarse resolution of the DWBC along steep sloping bottom and their greater dependence on the contribution of the bottom triangle transport.

The calculated northward transport of the AABW in the DWBC increases

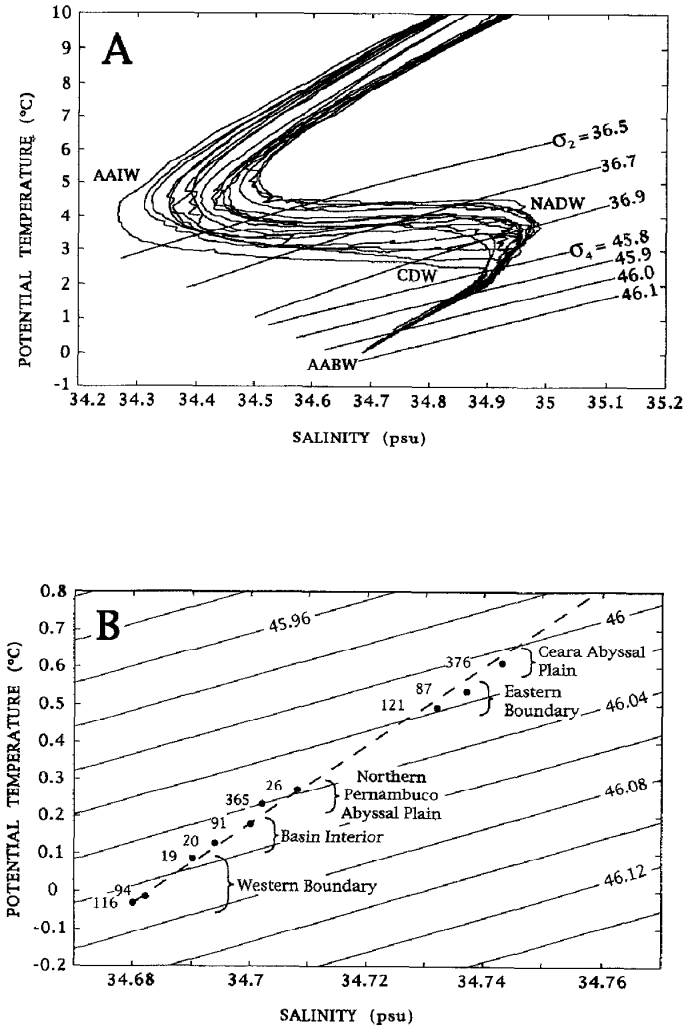

Figure 8. (A) Potential temperature-salinity diagram representative of the Brazil Basin. Isolines of potential density anomaly ($\sigma = \rho_{s,t,p} - 1000$ kg m^{-3}) are referred to 2000 dbar (σ_2) or 4000 dbar (σ_4). AAIW Antarctic Intermediate Water, NADW North Atlantic Deep Water, CDW Circumpolar Deep Water, AABW Antarctic Bottom Water. (B) Detail of the downstream evolution of the bottom potential temperature-salinity relationship for the AABW DWBC and for the circulation in the interior of the basin. The progressive warming and increasing salinity along the path of the AABW circulation matches the mean vertical θ-S relationship for AABW in the Brazil Basin indicated by a dashed line. Station locations are indicated in Figure 1.

downstream from 7.2 Sv near 24S, to 7.6 Sv near 19S, and to 7.9 Sv at 10S; however, due to problems with SAVE1 and SAVE3 noted in the previous paragraph the increase is probably not significant. The return flow, whose southward transport is about 5.0 Sv in the northern half of the basin, reduces to about 3.0 Sv at 25S. The

northward transport on the eastern side of the basin amounts to about 2.0 Sv. The transport estimates in the northern part of the Pernambuco Abyssal Plain indicate a large anticyclonic flow centered near 5S–25W. The transport estimates of this abyssal gyre vary from 3.0–5.0 Sv along the SAVE6 section to about 12.0–14.0 Sv along the SAVE1 section. The bulk of water denser than $\sigma_4 = 46.01$ kg m^{-3} contributes to more than two thirds of the total AABW transport, suggesting an intense activity of the bottommost circulation in this region. The northward net transport of AABW across the whole basin decreases from about 6.3 Sv along the SAVE3 ($\approx$24– 29S) section down to 4.4 Sv along the SAVE2 section ($\approx$ 15–19S).

The most reliable transport estimate, which occurs along the SAVE2 section, shows that the flow of WSDW, water denser than $\sigma_4 = 46.04$ kg m^{-3}, and the flow of water denser than $\sigma_4 = 46.01$ kg m^{-3}, the maximum density which can escape the basin (McCartney, 1994), amount to 2.0 Sv and 3.8 Sv respectively. Thus these dense water layers contribute respectively about one quarter and one half of the AABW DWBC transport. The maximum transport of AABW water lighter than $\sigma_4 = 46.01$ kg m^{-3} ($\approx$ shallower than 4500 m) entering directly the Ceara Abyssal Plain along the western boundary is estimated to be 1.5 Sv (DWBC transport minus return flow transport at 10S). Then an additional flow of about 2.5–3.5 Sv is required to match the 4.0–5.0 Sv cross-equatorial AABW transport estimated by McCartney and Curry (1993). Moreover, about 2.0 Sv of AABW warmer than 0.8°C transits the Mid-Atlantic Ridge through the Romanche Fracture Zone (Warren and Speer, 1991). As the AABW DWBC supply of water lighter than $\sigma_4 = 46.01$ kg m^{-3} is about 3.8 Sv, a supply of 2.0–3.0 Sv issued from the alteration (increase by mixing of its temperature and salinity) of denser water is necessary to balance the 6.0–7.0 Sv that exit the Brazil Basin.

c. Upward transport and cross-isopycnal mixing The time required to change the characteristics of the water denser than $\sigma_4 = 46.01$ kg m^{-3} confined to the deep Brazil Basin is equivalent to the time needed to flush this water out of the deep basin. For water denser than $\sigma_4 = 46.01$ kg m^{-3}, considering an inflow of 3.8 Sv and a volume in the Brazil Basin of about 2.25 10^{15} m^3 yields an approximate residence time of 19 years. This residence time is similar to the travel time of a water parcel flowing at 1 cm s^{-1} along the meandering path of the AABW circulation in the Brazil Basin (about 7000 km). Spread out uniformly over the area of the 46.01 kg m^{-3} isopycnal, about 4.5 10^{12} m^2, the out (upward) flow across the $\sigma_4 = 46.01$ kg m^{-3} isopycnal area yields an upwelling velocity of 8.5 10^{-7} m s^{-1}, which is comparable to the 3–4 10^{-7} m s^{-1} estimate of Hogg *et al.* (1982).

The variations of the upwelling intensity between the western and the eastern sides of the basin were estimated by looking at the different closed regions of the basin delimited by the hydrographic sections (Fig. 1). Cross-isopycnal flows of water, heat and salt were obtained by requiring the residual mass transport to balance below the different isopycnal surfaces in the AABW. The additional geothermal flux

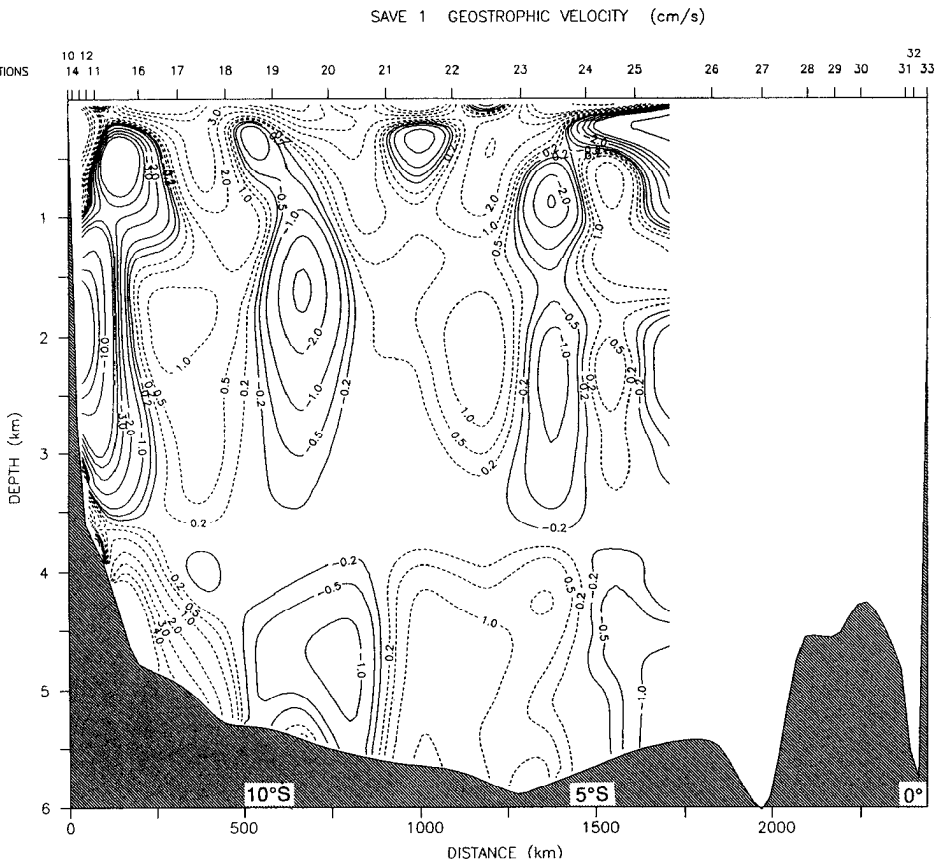

Figure 9. Contours of unfiltered geostrophic velocity (cm/s) along the different sections (A) SAVE1, (B) SAVE2, (C) SAVE3 and (D) SAVE6 (HYDROS4). The LNM is taken along the σ_4 = 45.87 kg m^{-3} isopycnal and along the bottom where this isopycnal is absent. Positive dashed isolines indicate northward (westward) flow, negative solid isolines indicate southward (eastward) flow.

from the seabed taken to be 4.2 10^{-2} W m^{-2} contributed only slightly to the warming of AABW. The southern part of the basin (boxes B and C) is characterized by an upwelling of cold/fresh AABW. Spread out uniformly over the area of the 45.87 kg m^{-3} isopycnal, about 1.68 10^{12} m^2 on the southwestern side of the basin (box B) and 1.20 10^{12} m^2 on the southeastern side (box C), this upwelling yields to cross-isopycnal velocities of 8.5 10^{-7} m s^{-1} and 4.1 10^{-7} m s^{-1} respectively. Variation of the reference level by $\pm$0.03 kg m^{-3} leads to differences in the upwelling velocity of less than $\pm$50% on the western side of the basin, but up to 300% on its eastern side. The mean upwelling velocity between the SAVE3 and SAVE2 sections (combining boxes B and C) is 6.4 10^{-7} m s^{-1}, with variations less than 70%.

Divergence across the lateral boundaries is indicated in upper layers of AABW in the northwestern part of the basin (box A), due mainly to an increase of the flow

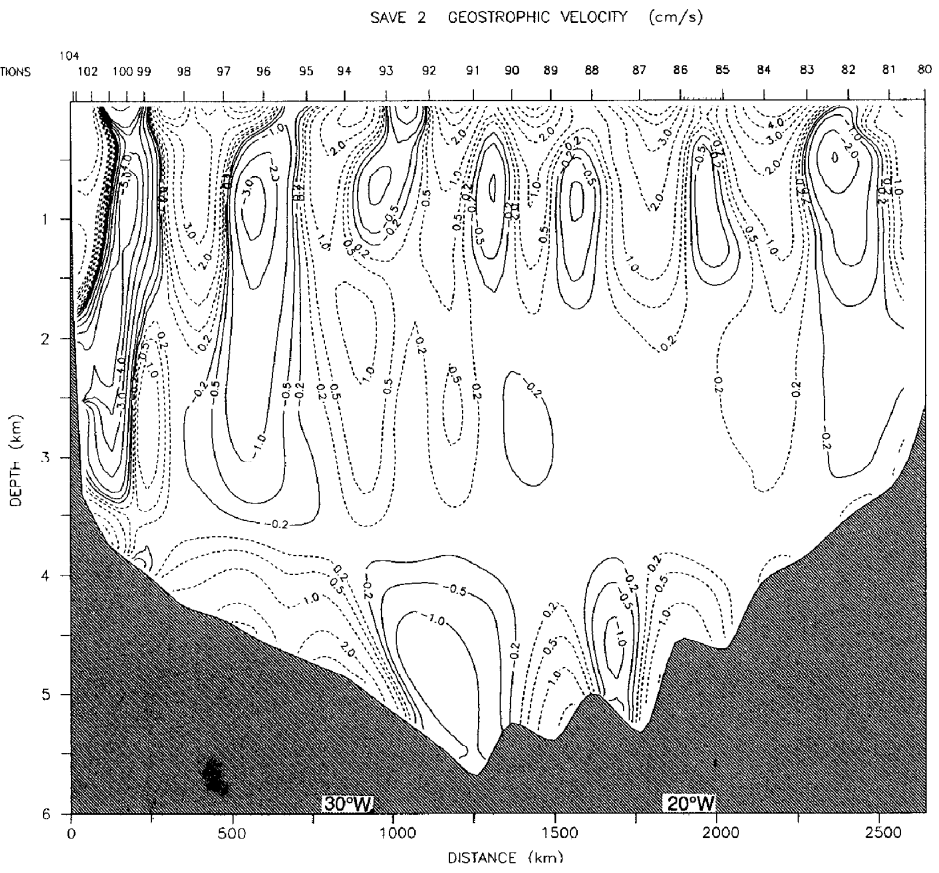

Figure 9. (Continued)

along the western boundary between σ_4 = 46.04 kg m^{-3} and 46.02 kg m^{-3}. The reliability of this divergence is doubtful due above all to the large outflow within the abyssal gyre in the northern Pernambuco Abyssal Plain. The transport of this gyre is three time stronger for SAVE1 than for SAVE6. The fact that box A includes only the western half of the gyre leads to a large unbalanced outflow of 10 Sv. However, the downstream vanishing of the densest layer of AABW ($\sigma_4 \geq$ 46.05 kg m^{-3}) north of 19S allows an estimation of the upwelling velocity within the DWBC that is 12.1 10^{-7} m s^{-1} for an isopycnal area of 0.95 10^{12} m^2. Thus it appears that the AABW in the southern part of the basin and along the western boundary are upwelled at a rate ranging between 1.7 10^{-7} m s^{-1} and 12.3 10^{-7} m s^{-1}. The larger values appear along the western boundary and for the densest layers of AABW in particular.

It seems reasonable, considering the apparent stability of the AABW density structures in the Brazil Basin, to assume a steady state between an upward advection of heat and salt and a mixing by diffusion of these properties across the isopycnals. In a study of the mixing of AABW above the Ceara Abyssal Plain, McDougall and

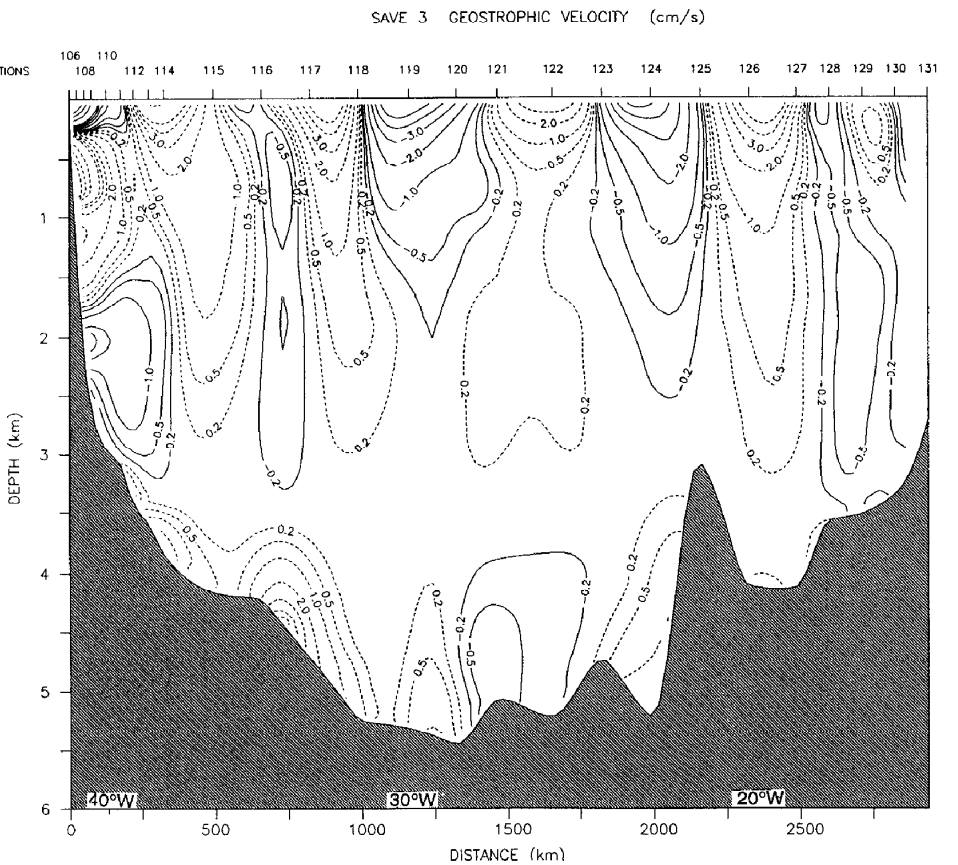

Figure 9. (Continued)

Whitehead (1984) envisaged the influence of three mixing processes: diapycnal salt fingering and turbulence, and isopycnal turbulence. They considered what the density flux ratio $R_f \equiv \alpha Q_\theta / \beta Q_s$ would be if one of these processes dominated, where α is the thermal coefficient of expansion, Q_θ is the vertical flux of heat, β is the saline contraction coefficient, and Q_s is the vertical flux of salt. If salt fingering dominated, they concluded, based on laboratory results of Schmitt (1979) and McDougall and Taylor (1984), that R_f should be close to 0.7. If diapycnal turbulence dominated they estimated that R_f should be

$$R_f = (\alpha k_\theta \partial\theta/\partial z)/(\beta k_s \partial S/\partial z),$$

where k_θ and k_s are the turbulent diapycnal diffusivities for heat and salt, respectively. Assuming that this turbulence should mix heat and salt at about the same rate ($k_\theta \approx k_s$), they concluded that

$$R_f \approx (\alpha \partial\theta/\partial z)/(\beta \partial S/\partial z).$$

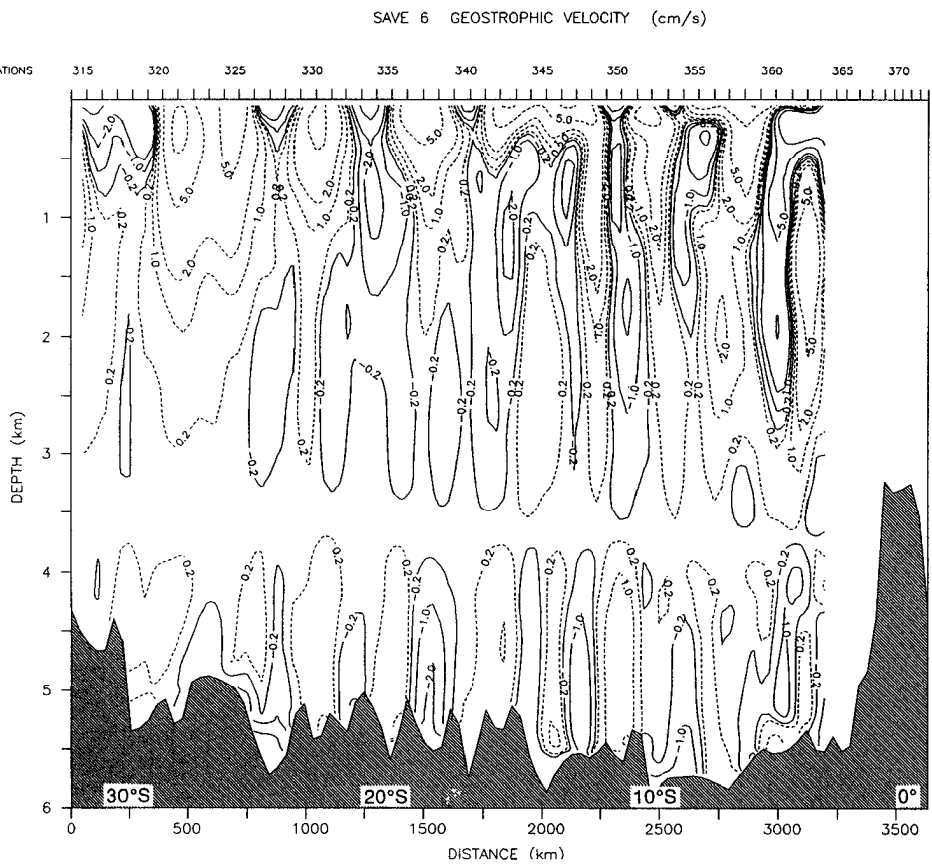

Figure 9. (Continued)

This last relation is also the density ratio R_ρ, which for the deep Brazil Basin is about 2.2–2.6. If isopycnal turbulence dominated they estimated that R_f across an isothermal surface should be

$$R_f = (\alpha K_{i\theta} \nabla_i \theta)/(\beta K_{iS} \nabla_i S),$$

where $K_{i\theta}$ and K_{iS} are the isopycnal diffusivities for heat and salt, respectively, ∇_i is the two-dimensional gradient in the isopycnal plane. Assuming that the isopycnal diffusivities were nearly equal, and noting that along an isopycnal surface $\alpha \nabla_i \theta = \beta \nabla_i S$, they concluded that this last relation should reduce to

$$R_f \approx 1.$$

In summary they concluded that R_f should be about 0.7, R_ρ or ≈ 1 if, respectively, salt fingering, diapycnal diffusion, or isopycnal diffusion were the dominant mixing process.

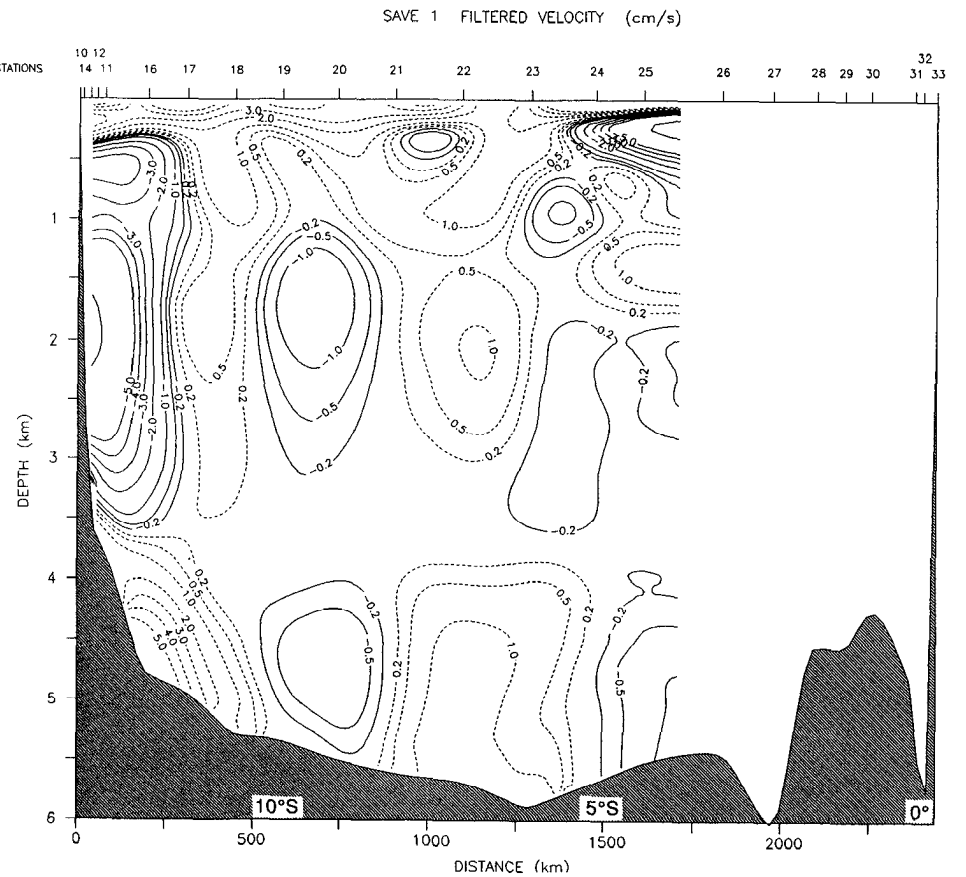

Figure 10. Contours of filtered geostrophic velocity (cm/s) along the different sections: (A) SAVE1, (B) SAVE2, (C) SAVE3 and (D) SAVE6 (HYDROS 4). The LNM is taken along the $\sigma_4 = 45.87$ kg m^{-3} isopycnal and along the bottom where this isopycnal is absent. Positive dashed isolines indicate northward (westward) flow, negative solid isolines indicate southward (eastward) flow.

Estimates of the density flux ratio in the southern basin (boxes B and C in Fig. 1) indicate, following McDougall and Whitehead (1984), that diapycnal turbulent mixing is the dominant mixing process (Fig. 13). The diffusion rates at which heat and salt from the warm and salty NADW mix with colder and fresher AABW range from 3.6 10^{-4} m^2 s^{-1} to 7.2 10^{-4} m^2 s^{-1}. The larger values appear in the southeastern part of the basin (box C in Fig. 1) where the vertical gradient of properties are smaller.

d. Bottom layers

The DWBC bottom layers. The previous discussion of the NADW DWBC suggests that its bottom layer is slippery, denser than a flat bottom layer (i.e., too dense) and stratified, and that it thickens downstream. The geostrophic current estimates

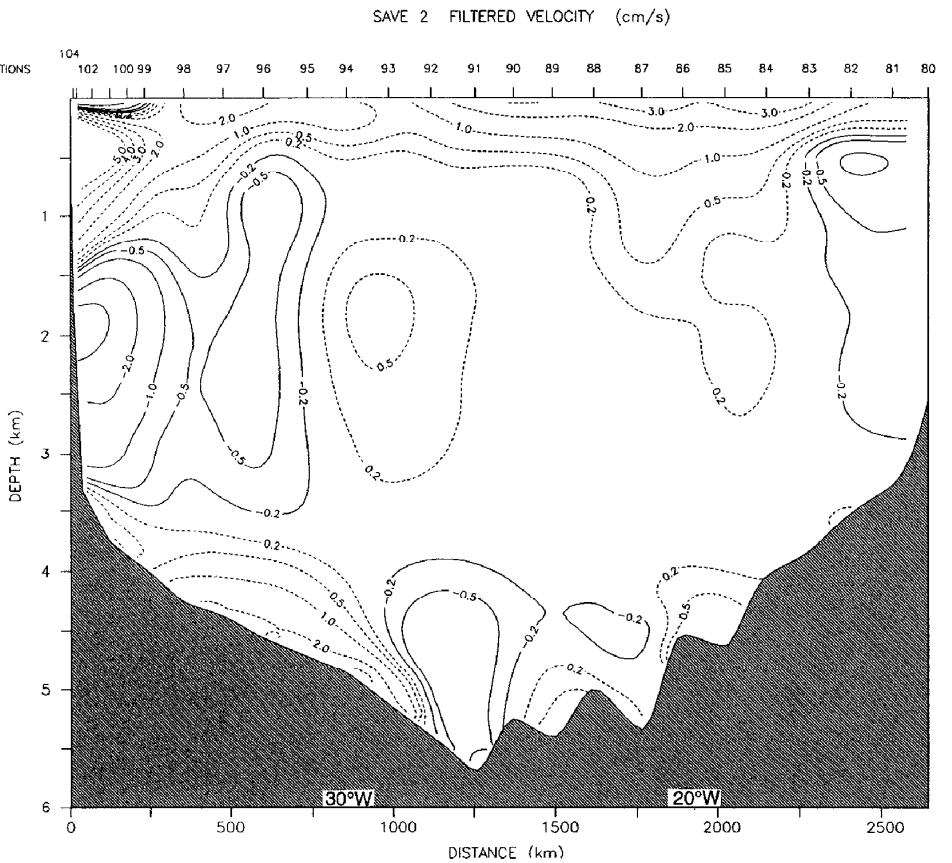

Figure 10. (Continued)

(Fig. 9A–C) indicate that the maximum flow for this DWBC is in UNADW-MNADW and has a strength of about 5–20 cm s^{-1}. Each of the zonal SAVE sections has a station where the UNADW-MNADW is in contact with the bottom. These stations indicate too dense stratified bottom layers (in one case with a remnant BML just above the bottom) which thicken downstream (Fig. 14). With $\alpha \approx 0.08, 0.03$ and 0.01 for the SAVE1 #14, SAVE2 #104 and SAVE3 #108 stations, respectively, Eq (1) with $\Delta\rho$ inferred from Figure 14, gives a thermal wind reduction for velocity $\Delta V \approx$ 15–25 cm s^{-1}. All of the above indicate that the bottom layer of the NADW DWBC is slippery.

The bottom layers of the NADW DWBC are rather thick ($\approx$ 110 m at 11S, $\approx$ 120 m at 18S and $\approx$ 240 m at 23S; Fig. 14). This is thicker than we expected; the upwelled bottom layer thicknesses shown in Weatherly and Martin (1978), Trowbridge and Lentz (1991) and MacCready and Rhines (1993) are nearly an order of magnitude thinner. However, this may not be unusual because these layers were probably formed near the equator where f is small. As noted earlier, a newly formed upwelled

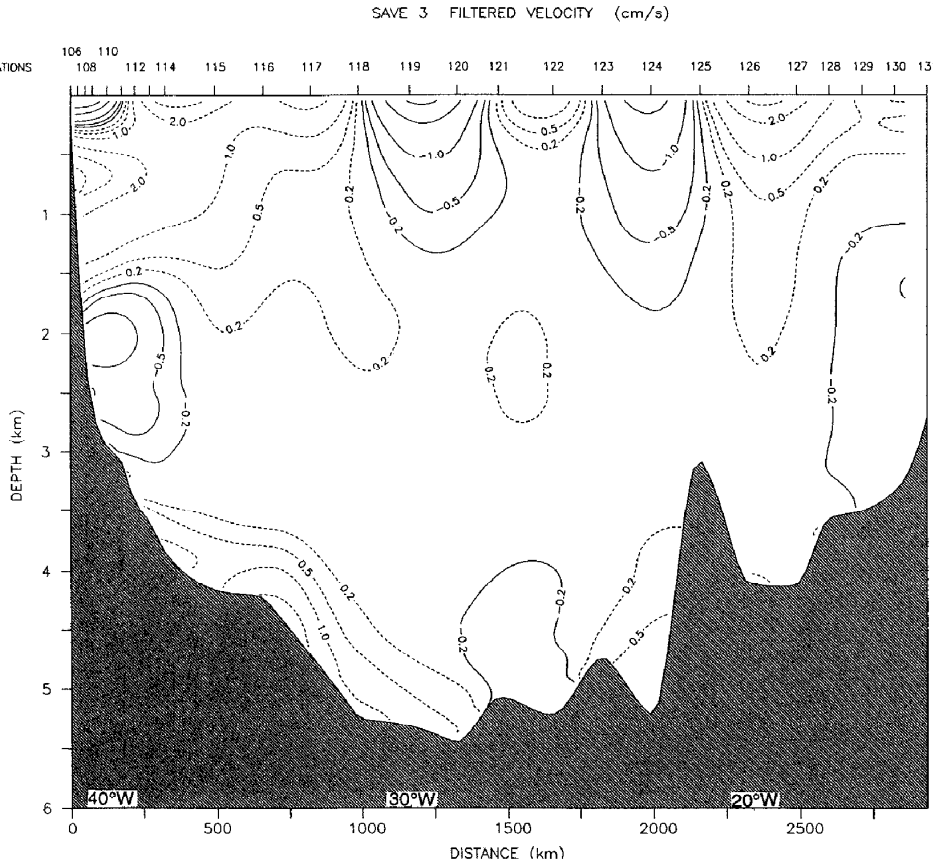

Figure 10. (Continued)

bottom layer should be about as thick as a bottom layer formed over a flat bottom. Weatherly and Martin (1978) proposed that this later thickness should be about

$$h = 1.3\, u_* |f^{-1}| \{1 + N^2 f^{-2}\}^{-1/4} \tag{3}$$

where u_* is the square root of the bottom stress divided by density. Taking u_* to be about 4% of the flow above the bottom layer (ibid.), the flow above the bottom layer to be about 15 cm s^{-1}, $N = 1.7 \times 10^{-3}$ s^{-1}, and $f = -0.5 \times 10^{-5}$ s^{-1} (latitude about 2S) gives

$$h = 85 \text{ m}.$$

This is close to the observed 110 m thickness at the northernmost section SAVE1 (Fig. 14).

The previous discussion about the bottom layer of the AABW DWBC suggests that downslope advection should have a noticeable effect on the layer but that it

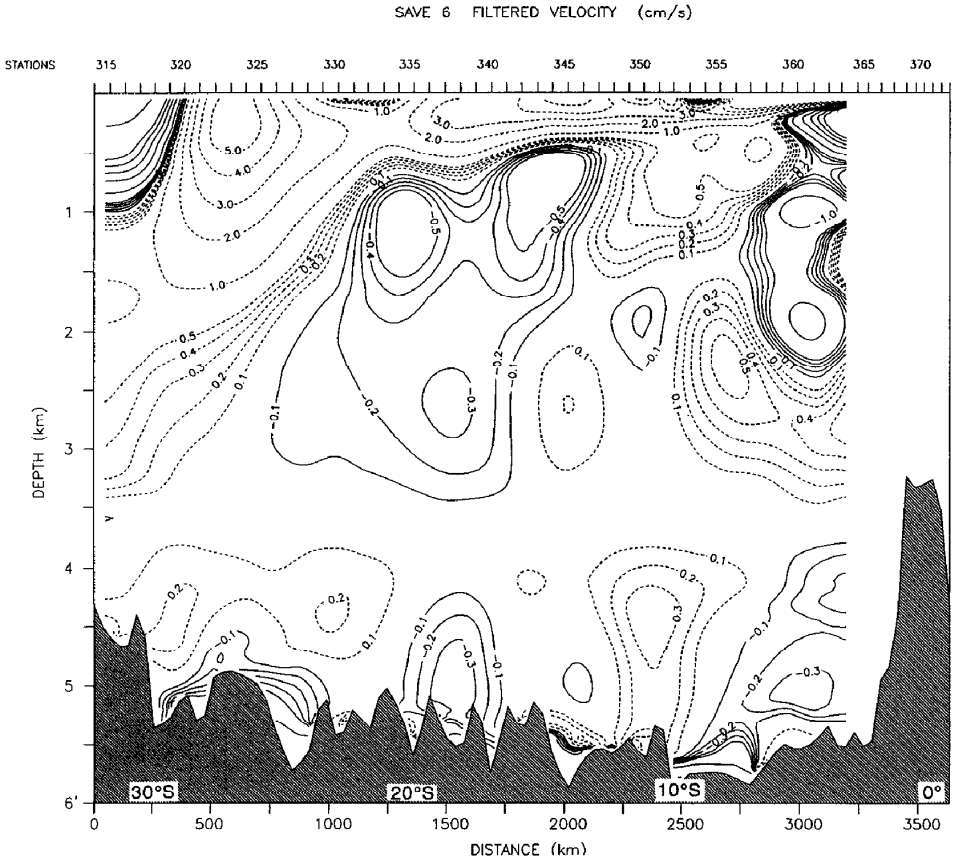

Figure 10. (Continued)

Table 1. Potential density surfaces used to define the water mass layers. CDW, Circumpolar Deep Water; NADW, North Atlantic Deep Water; AABW, Antarctic Bottom Water; WSDW, Weddell Sea Deep Water.

Layer	Upper isopycnal	Lower isopycnal
NADW	$\sigma_2 = 36.70$ kg m^{-3}	$\sigma_4 = 45.87$ kg m^{-3}
Upper NADW	$\sigma_2 = 36.70$ kg m^{-3}	$\sigma_2 = 36.95$ kg m^{-3}
Middle NADW	$\sigma_2 = 36.95$ kg m^{-3}	$\sigma_2 = 37.02$ kg m^{-3}
Lower NADW	$\sigma_2 = 37.02$ kg m^{-3}	$\sigma_4 = 45.87$ kg m^{-3}
AABW	$\sigma_4 = 45.87$ kg m^{-3}	Bottom
Lower CDW	$\sigma_4 = 45.87$ kg m^{-3}	$\sigma_4 = 46.04$ kg m^{-3}
WSDW	$\sigma_4 = 46.04$ kg m^{-3}	Bottom

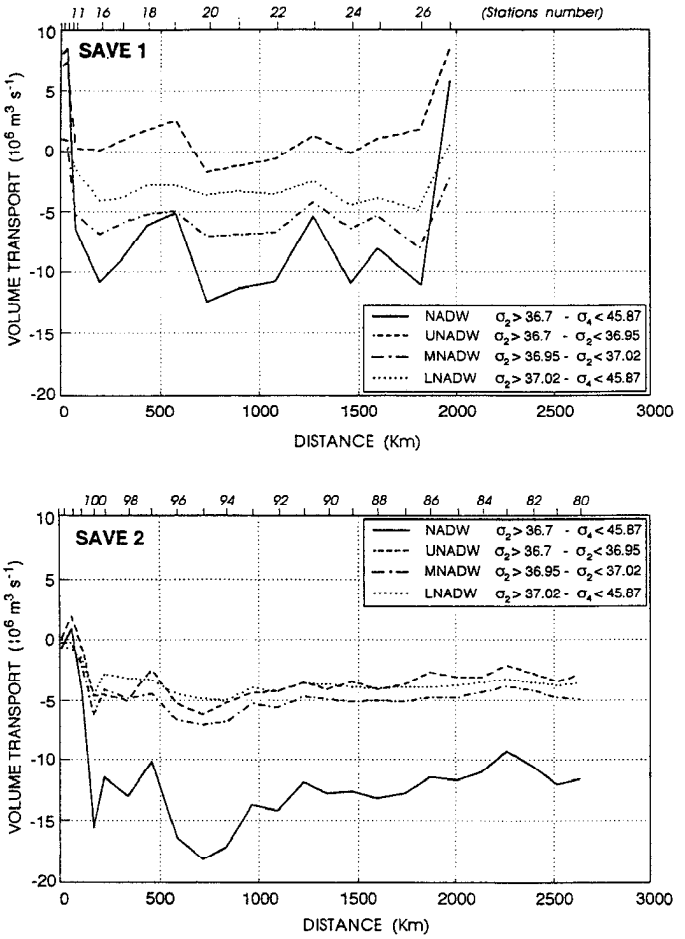

Figure 11. Cumulative geostrophic transports of NADW and its components along the different sections: (A) SAVE1, (B) SAVE2, (C) SAVE3 and (D) SAVE6 (HYDROS4). Negative transport indicates southward (eastward) integrated flow.

should be insufficient to result in a slippery bottom layer. A comparison of the density sections in Figure 5 shows a fundamental difference in the AABW DWBC from that of the NADW DWBC in that in the former the water density does not monitonically increase with depth along the bottom. A further complication results because the high density core of the AABW only coincides with the AABW DWBC in the SAVE3 and SAVE2 sections (Figs. 5 and 10). We will first consider these two SAVE sections before considering the SAVE1 section.

Upslope of and in the vicinity of the high density core in the SAVE3 and SAVE2 sections (Figs. 5B,C and 10B,C) downslope advection should result in too light bottom layers in the AABW DWBC. This was the case in all the density profiles

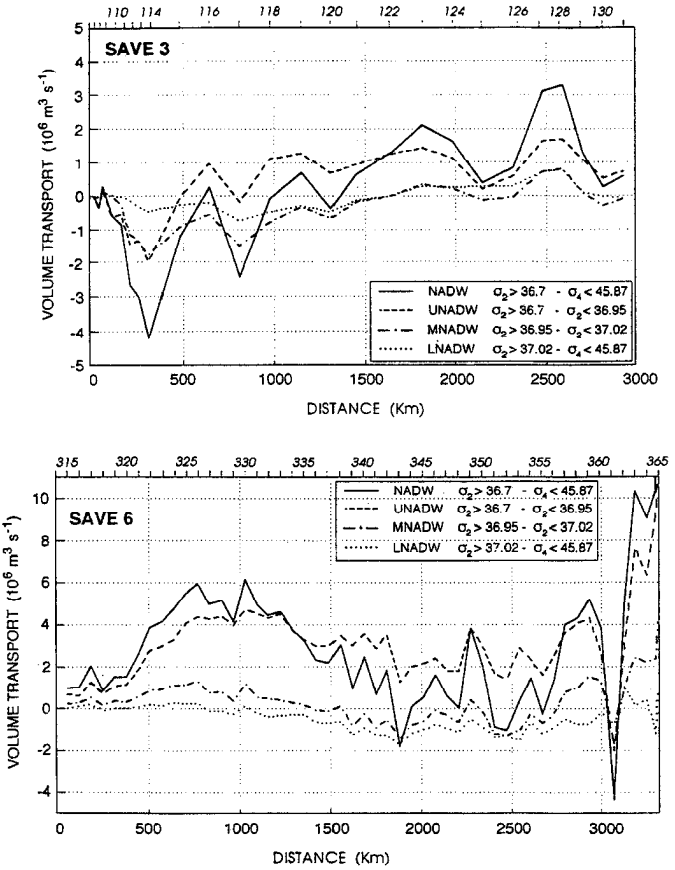

Figure 11. (Continued)

examined (e.g., Fig. 15A,B). Further, in this region the BML should be thicker than that of a level bottom BML and should thicken downstream. Using Eq. (4), taking the AABW DWBC flow to be about 5 cm s^{-1} (Figs. 10B,C) and u_* 4% of it, and using values of f and N previously used for this DWBC yields a level-bottom BML thickness of about 15 m. The observed BML thicknesses in this region varied from 40 m to 110 m (e.g., Fig. 15A,B). The BML thickness also increased going downstream in this region (Fig. 16). We estimated the density anomaly due to cross-slope advection $\Delta\rho$ to be the observed BML density relative to that of level-bottom BML thickness of 15 m (cf. Fig. 15A,B). The ΔV estimated from Eq. (1) using these $\Delta\rho$s were all less than 1 cm s^{-1} which is much less than the 5 cm^{-1} flow rate of this DWBC (Fig. 10B,C). This reinforces the earlier inference that the bottom layer of the AABW DWBC (at least in this region) is only partially slippery. Downslope of the high density core, across-slope advection should result in too dense bottom layers, and in general this was indeed observed (e.g., Fig. 15C). Interestingly, the resultant

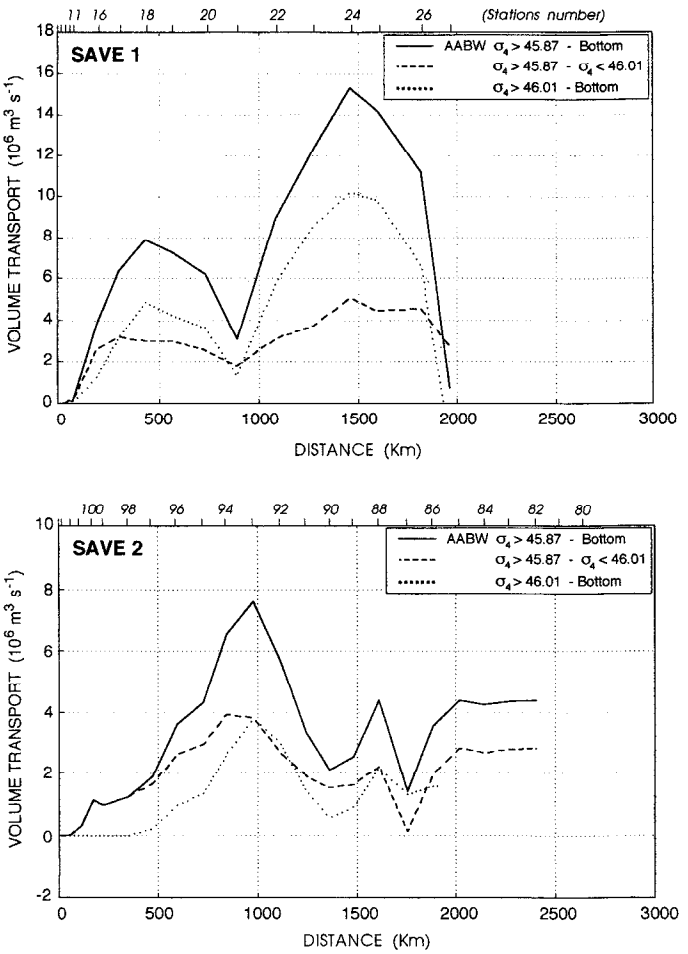

Figure 12. Cumulative geostrophic transports of AABW along the different sections: (A) SAVE1, (B) SAVE2, (C) SAVE3 and (D) SAVE6 (HYDROS4). A separation is made between the waters confined in the deep basin (σ_4 > 46.01 kg m^{-3}) and the overlying waters. Positive transport indicates northward (westward) integrated flow.

thermal wind change ΔV (cf. Eq. 1) though small (about 1 cm s^{-1} or less) now acts to accelerate the flow across the bottom layer. Thus downslope of the high density core advection in the bottom layer tends to make the layer more frictional rather than slightly slippery!

Somewhere between the SAVE2 AND SAVE1 sections the AABW DWBC diverges from the high density core because this high density core, as previously noted, cannot exit the basin. Because of this we expect the bottom layer to be thinner at the SAVE1 section compared to the SAVE2 section and this was indeed the case

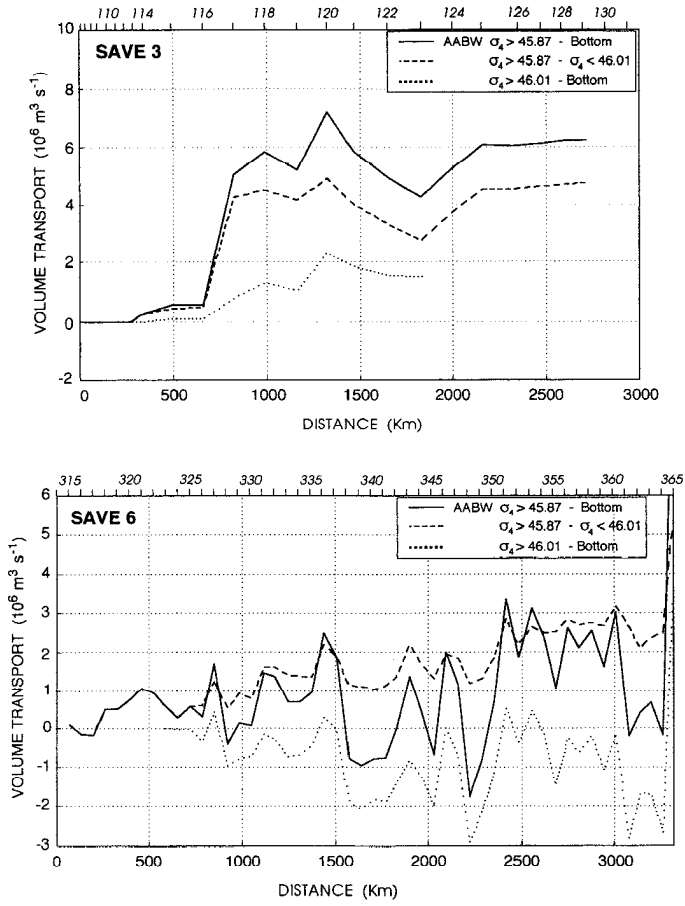

Figure 12. (Continued)

(e.g., Figure 15B,D). We would expect it to be thicker than 15 m and to be too light; and this was in general what was observed (e.g., Fig. 15D).

Thick homogeneous layer of WSDW in the northern Pernambuco Abyssal Plain. Besides the bottom layers along the sloping western boundary, well developed homogeneous layers extending 200 to 600 m above the bottom appear in the northern part of the Pernambuco Abyssal Plain where the sea floor is deeper than 5400 m (Fig. 17). The water in these layers shows a density of about 46.044 kg m^{-3} and a slight increase in oxygen, which is probably characteristic of WSDW. The bulk of WSDW is trapped within the northern Pernambuco Abyssal Plain because there is no exit further south where the seafloor rises. This water is not stagnant; the superposition of the hydrographic properties with the cyclonic gyre suggests a highly active abyssal circulation. The structure of the flow (cyclonic gyre) is compatible with a conver-

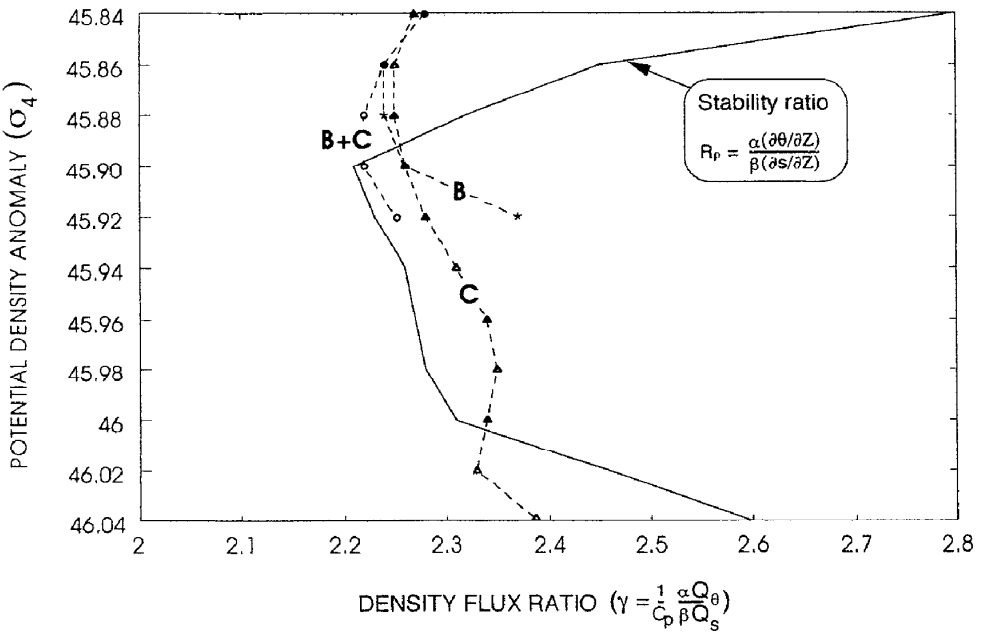

Figure 13. Vertical evolution of density flux ratios in the different boxes. The solid line characterizes the density (or stability) ratio.

gence in the bottom layer and a subsequent upwelling of WSDW in the interior. Peggion and Weatherly (1991) have shown that such upwelling can lead to homogeneous bottom layers much thicker than expected from expression (3).

6. Summary and conclusions

a. Circulation of NADW

The NADW circulation we infer is sketched in Figure 18. Several deep anticyclonic gyres are traced along the Brazil slope. The recirculations along the northern Brazilian slope north of 19°S are consistent with the results of McCartney (1993). McCartney first established the existence of anticyclonic recirculations immediately offshore the DWBC. We show that these abyssal gyres appear rather to be nested within a broader DWBC that extends about 800 km offshore. The latitudinal

Figure 14. Profile of potential density anomaly (referred to 2000 dbar) in the core of the southward-flowing NADW DWBC near (A) 10S (station 14), (B) 19S (station 104) and (C) 24S (station 108). The abscissa is positioned at the bottom depth. The dashed line characterizes the density profile in the absence of any upwelling. The dashed bottom mixed layer was drawn so the extrapolated, dotted profile bisects it. $\Delta\sigma$ indicates our estimate of the density anomaly across the bottom layer resulting solely from the upslope advection of denser water. The casts in (A), (B) and (C) were terminated at 28 m, 10 m and 8 m above the bottom, respectively.

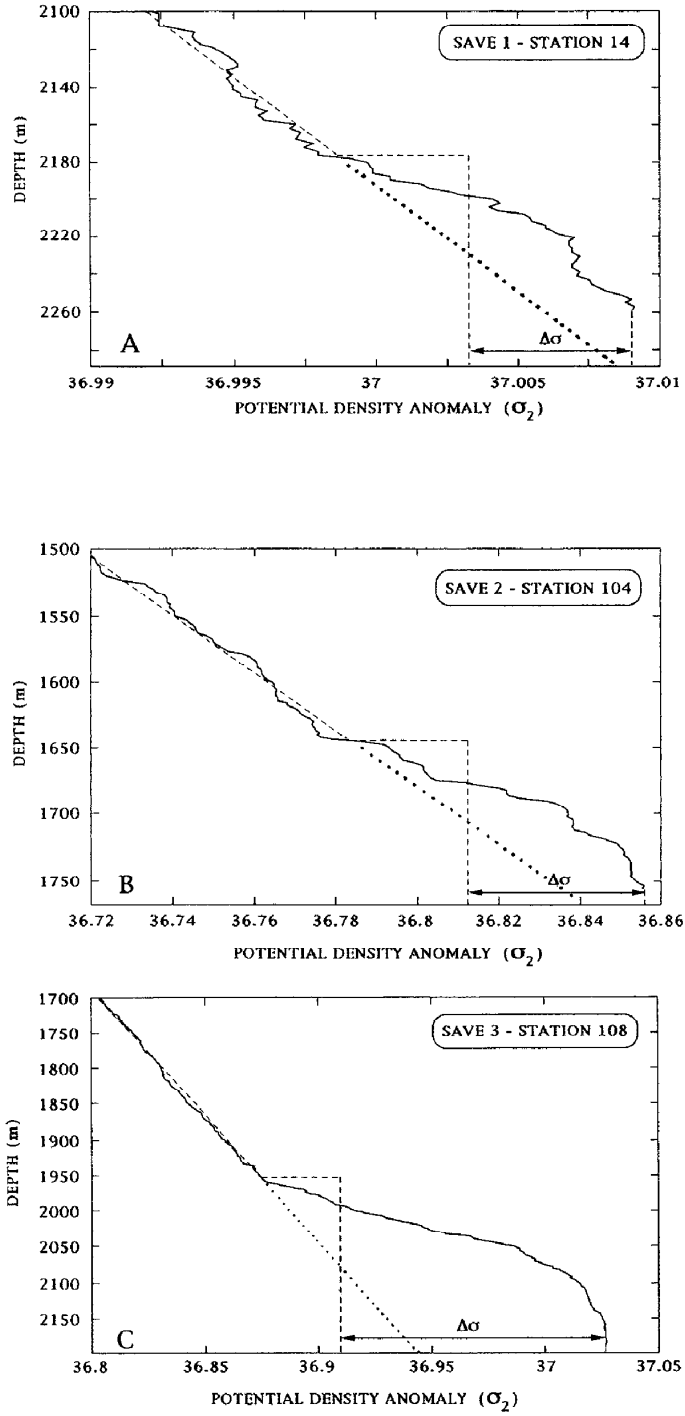
SAVE 1 - STATION 14
DEPTH (m)
2100
2140
2180
2220
2260
A
Δσ
36.99
36.995
37
37.005
37.01
POTENTIAL DENSITY ANOMALY (σ2)
SAVE 2 - STATION 104
DEPTH (m)
1500
1550
1600
1650
1700
1750
B
Δσ
36.72
36.74
36.76
36.78
36.8
36.82
36.84
36.86
POTENTIAL DENSITY ANOMALY (σ2)
SAVE 3 - STATION 108
DEPTH (m)
1700
1750
1800
1850
1900
1950
2000
2050
2100
2150
C
Δσ
36.8
36.85
36.9
36.95
37
37.05
POTENTIAL DENSITY ANOMALY (σ2)

Figure 14

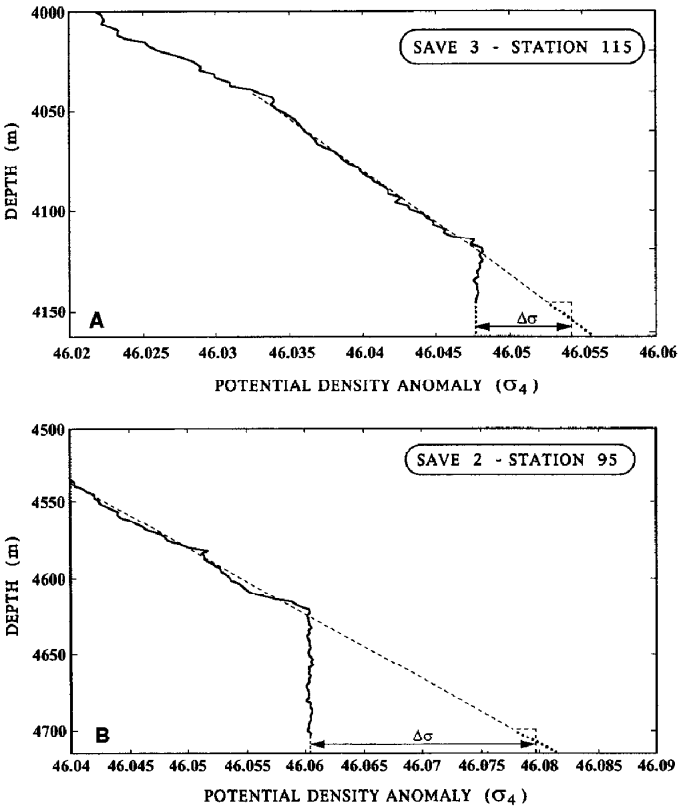

Figure 15. Examples of bottom layers from the AABW DWBC. The dashed profiles extrapolated from the overlying water are our estimates of how the profile would look for a bottom layer formed over a level bottom, and $\Delta\sigma$ is our estimate of the density anomaly due to across-slope advection. (A) and (B) are from upslope of the high density core for the SAVE3 and SAVE2 sections, respectively. In these sections the high density core of AABW coincides with the DWBC. These layers are too-light, exceptionally thick BMLs (i.e., they are less dense and thicker than the BML expected to form over a level bottom). (C) is from downslope of the high density core in the SAVE3 section and shows a too-dense bottom layer. (D) is from the SAVE1 section where the high density core no longer coincides with the DWBC (see text).

extension of these recirculations appears to be limited by bathymetric features implying large changes in the direction of the slope. McCartney (1993) described two recirculation gyres north of 16S, one centered over the Demerara Abyssal Plain north of the equator, and another near 11S. However, the degree of their connection was uncertain. The results from the SAVE data set confirm the existence of an anticyclonic abyssal gyre between 10S and 19S. Furthermore, they imply that this recirculation must be disconnected from that further north in order to permit the passage of the eastward-flowing branch of NADW that separates from the DWBC at the latitude of Cape Saõ Roque ($\approx$5S). Likewise, the recirculation south near 24S

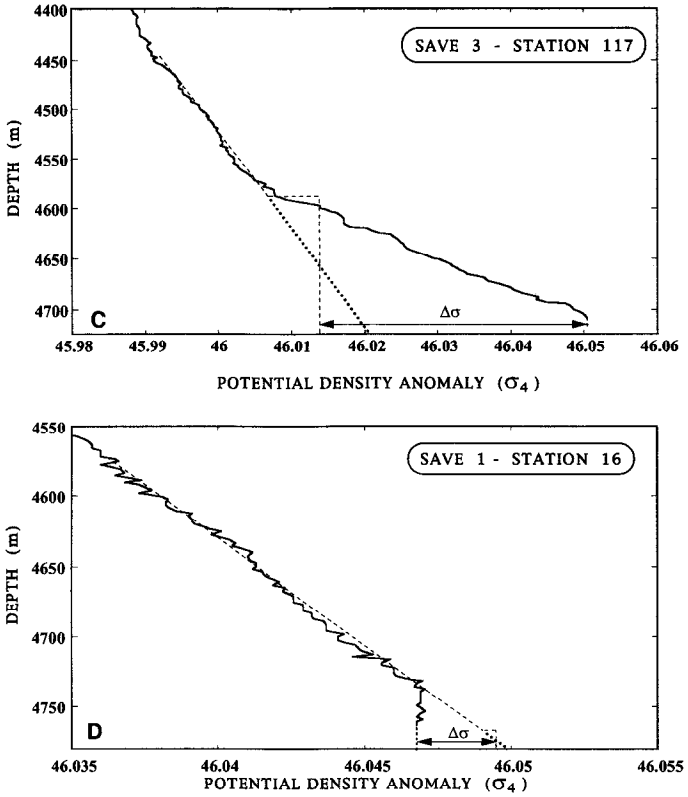

Figure 15. (Continued)

must be disconnected from the recirculation gyre north of 20S to allow the branch of the NADW DWBC, where it bifurcates at the latitude of the Columbia-Trinidad Seamount Chain, to flow towards the interior of the basin. We suggest that the northernmost recirculation gyre over the Ceara Abyssal Plain should extend eastward as far as the mid-longitude of the basin to include the westward counterflow of UNADW and MNADW observed near 8S.

The northern branch of NADW flowing eastward close to the equator and entering the Brazil basin at low latitudes is consistent with the observations of Wüst (1935), Weiss *et al.* (1989), Ponte *et al.* (1990) and Tsuchiya *et al.* (1994). The overall NADW flow patterns in the interior of the basin are consistent with the descriptions of the circulation given by Defant (1941), Reid (1989), Zhang and Hogg (1992) and Tsuchiya *et al.* (1994). The net southward flow across the basin at 19S is estimated to about 11 Sv. This transport is consistent with McCartney's (1993) 12.5 Sv at 11S. Nevertheless, the transports of the inner branch of the DWBC and the recirculation in McCartney (1993), which amount to 34.0 Sv and 22.0 Sv respectively, are higher than our estimates of 19.3 Sv and 5.7 Sv, respectively, at 10S and of 19.0 Sv and 6.3 Sv, respectively, at 19S. The differences probably relate to the resolution of the fine

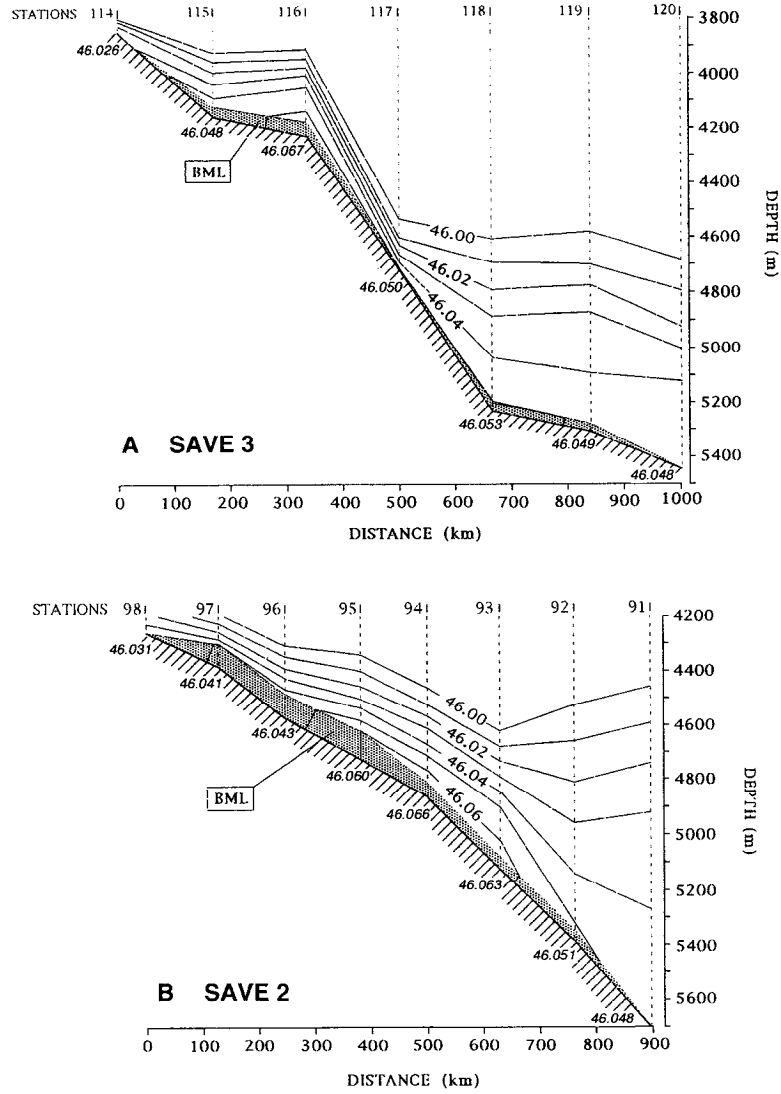

Figure 16. Contours of potential density anomaly (referred to 4000 dbar) in the core of the northward-flowing AABW DWBC near (A) 25S and (B) 18S. A bottom mixed layer (dashed region) characterizing the downslope advection of lighter water is evident along the bottom.

hydrographic structures, like the isopycnal dip near the lower slope, that are better defined in the sections considered by McCartney (1993). The contribution to the total transport of the three components of NADW are rather similar along the western boundary north of the Columbia-Trinidad Seamount. This represents a major difference from the results of Molinari *et al.* (1992) north of the equator, which show LNADW making a major contribution.

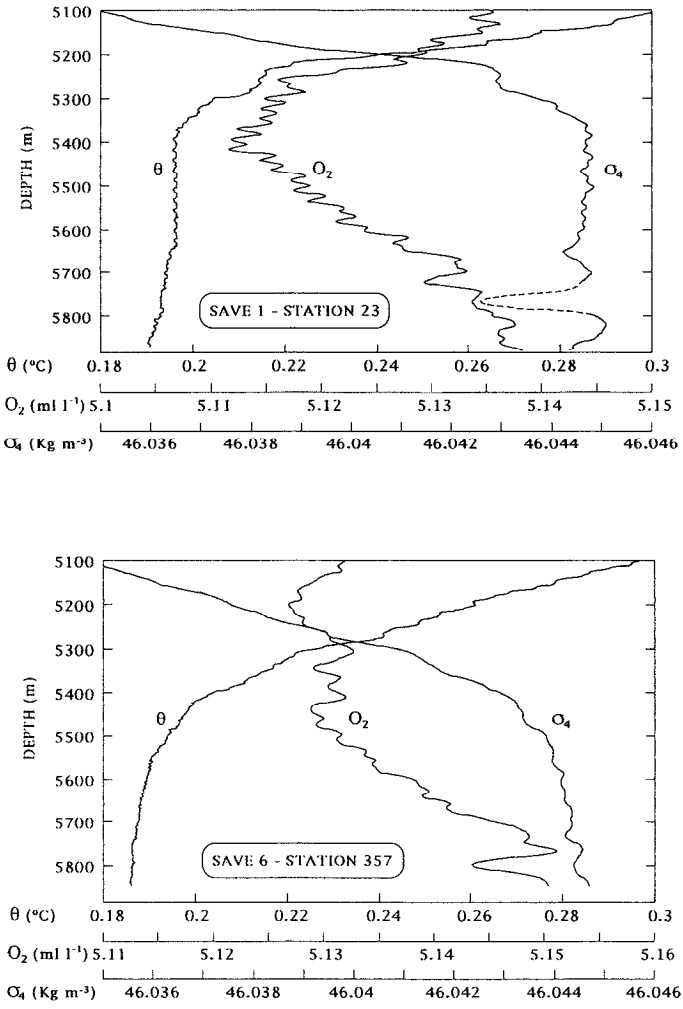

Figure 17. Profiles of potential temperature, (smoothed) oxygen and potential density anomaly (referred to 4000 dbar) in the northeastern Brazil Basin near 3S. A homogeneous layer of WSDW (denser than $\sigma_4 \approx 46.044$) is evidenced in the last 500 m of the water column.

b. Circulation of AABW

The path of AABW throughout the Brazil Basin that we infer from the SAVE data set is sketched in Figure 19. Contrary to the NADW circulation, the AABW is dominantly meridional and meanders around the topographic features that interrupt its path. The main patterns and the transports of the meridional AABW circulation are consistent with the description given by McCartney and Curry (1993) and Speer and Zenk (1993). In fact, with the exception of the topographic effects and the cyclonic gyre in the northern basin, our figure looks very similar to Figure 13 in Speer and Zenk (1993). The major features of the AABW circulation appear to be

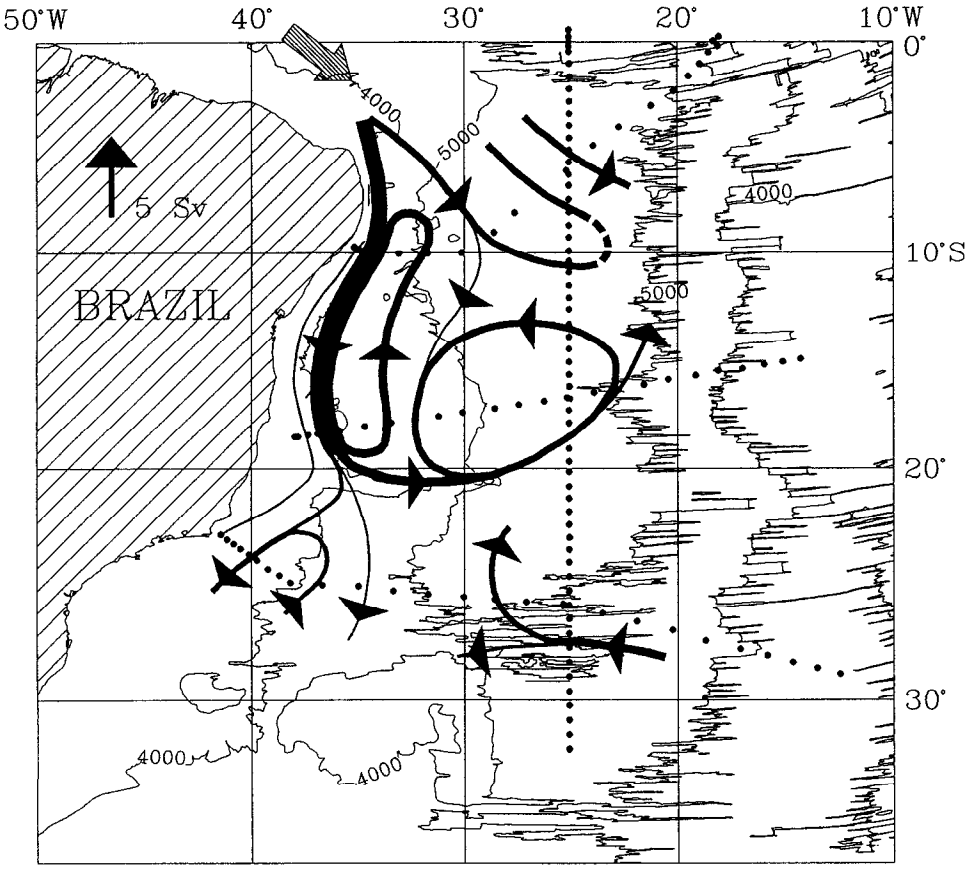

Figure 18. Sketch of the circulation of NADW in the Brazil Basin. Hatched arrows indicate in- and outflows inferred from others' studies. The thin line along the slope delineates the inner limit of the Deep Western Boundary Current.

characterized by (1) a northward-flowing DWBC, (2) a return flow immediately offshore of the DWBC that may contribute to a slight downstream increase of the DWBC transport and (3) a northward return flow in the eastern basin. In addition, new features are described, like the termination of the lens of dense AABW south of 25S in the mid-basin and a strong cyclonic abyssal gyre in the northern part of the basin composed of denser (o_4 > 46.01) AABW which cannot exit the Brazil Basin. The lower part of this gyre consists of WSDW. In the Ceara Abyssal Plain the AABW DWBC is only in part a direct continuation from the Brazil Basin. It is likely that a complementary flow of AABW enters the Ceara Abyssal Plain at some other location.

The upwelling velocities and the coefficients of diapycnal turbulent mixing in AABW, estimated from simple mass budgets, are reasonable and suggest that,

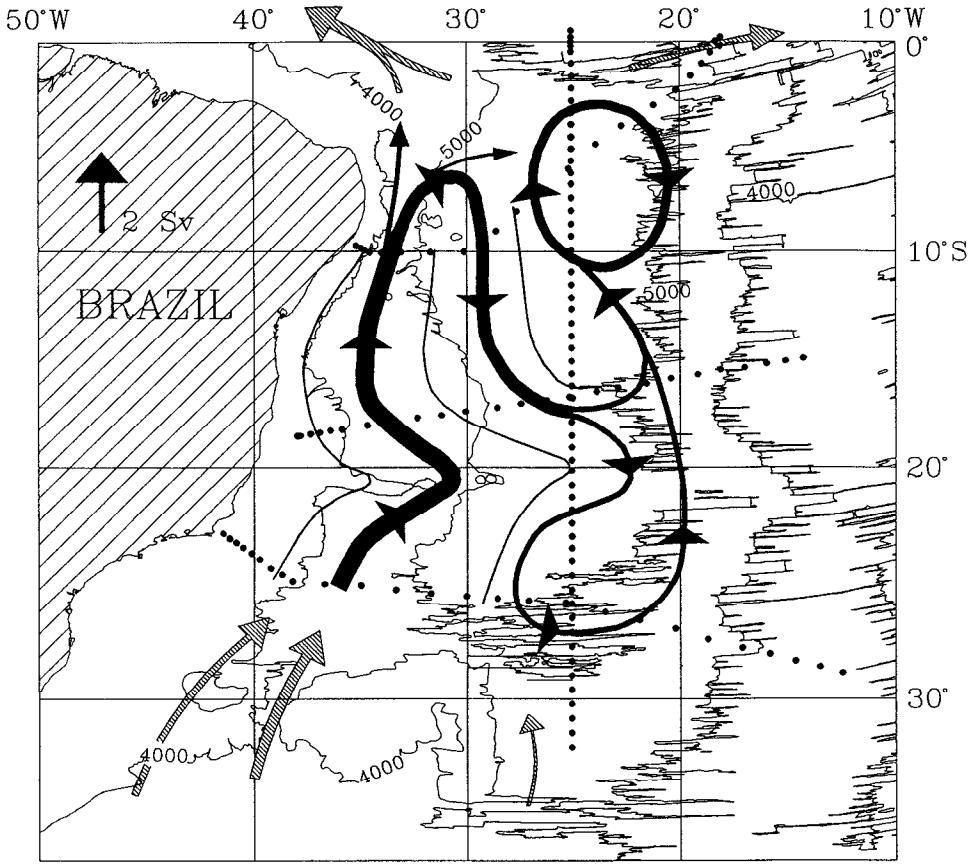

Figure 19. Sketch of the circulation patterns of AABW in the Brazil Basin. The hatched arrows indicates inflow inferred from others' studies. The thin lines delineate the limits of the Deep Western Boundary Current and the return flow.

compared to the interior of the basin, there is intensified mixing along the western boundary. The basin-wide values of these parameters are comparable to the estimates of Hogg *et al.* (1982) and Speer and Zenk (1993).

Implicit in our estimates is that the AABW properties did not change during the time period the SAVE sections were made. Coles *et al.* (1994) indicate that this was not strictly correct. Using the same SAVE data as well as other data they found a slight freshening and warming of AABW in the Brazil and Argentine Basin in the 1980's. They found these changes were more significant for waters colder than $\theta \approx 0.5$°C in the Brazil Basin. We think that inclusion of this temporal variability would not appreciably change our inferred estimates of vertical velocities and diapycnal diffusivities, and that it might change our inferred circulation path in the southern central basin; however, more work is needed to verify this.

c. Bottom boundary layers in the DWBCs

The bottom mixed layers of the DWBCs indicated the expected across-slope advection: upslope for the NADW DWBC and downslope for the AABW DWBC. The former appeared sufficient to make the bottom layer slippery. The latter appeared sufficient to create exceptionally thick (50 to 100 m) bottom mixed layers, but insufficient to make the bottom layer slippery.

The bottom layer for the NADW DWBC thickened downstream from about 110 m at 10S to about 220 m at 24S. Such a downstream thickening is consistent with the slow diffusion process for the spun-down bottom layer described in MacCready and Rhines (1993) with a vertical diffusivity of about 5 10^{-4} m^2 s^{-1}. This diffusivity is consistent with the abyssal diapycnal diffusivity estimated by another method in this study.

In conclusion, we do not mean to imply that our transport estimates are definitive nor that our estimated flow patterns are either. We have used rather standard choices of LNM to estimate transports and from these have attempted to infer flow patterns consistent with them using perhaps the finest hydrographic data set from the Brazil Basin. We have also made the standard assumption that the observations were synoptic when in fact they were not. We expect that subsequent observations made in the Brazil Basin will show that at least some of the assumptions and/or our conclusions will need major revision.

Acknowledgments. We benefited from conversations with William Smethie, Jr., and detailed comments from the reviewers. Support of this work was provided through NSF grant OCE92-06117, ONR contract N00014-92-J-1024 and DOE grant DE-FG05-92ER61416. One of the authors (XDDM) was partly supported by a postdoctoral fellowship of the Swiss National Science Foundation.

REFERENCES

Coles, V. J., M. S. McCartney, D. B. Olson and W. Smethie. 1994. Changes in Antarctic Bottom Water properties in the Western South Atlantic in the late 1980's. (in preparation).

Defant, A. 1941. Die absolute Topographie des Physikalischen Meeresniveaus und der Druckflashen sowie die Wasserbewegungen in Raum des Atlantischen Ozeans. Quantitative Untersuchungen zur Statik und Dynamik des Atlantischen Ozeans. Wissenschaftliche Ergebnisse der Deutschen Atlantischen Expedition auf dem Vermessungs-und Forschungsschiff "Meteor" 1925–1927, *6,* 191–260.

Fofonoff, N. P. 1985. Physical properties of seawater: a new salinity scale and equation of state for seawater. J. Geophys. Res., *90,* 3332–3342.

Fu, L. L. 1981. The general circulation and meridional heat transport of the subtropical South Atlantic determined by inverse methods. J. Phys. Oceanogr., *11,* 1171–1193.

Fuglister, F. C. 1960. Atlantic ocean atlas of temperature and salinity profiles and data from the International Geophysical Year of 1957–1958. Woods Hole Oceanographic Institution, Woods Hole, MA, 209 pp.

Garrett, C., P. MacCready and P. Rhines. 1993. Boundary mixing and arrested Ekman layers; rotating stratified flow near a sloping boundary. Ann. Rev. Fluid Mech., *25,* 291–323.

Hoffman, E. E. and S. J. Worley. 1986. An investigation of the circulation of the Gulf of Mexico. J. Geophys. Res., *91,* 14221–14236.

Hogg, N. G. 1990. Towards a Deep Basin Experiment. WOCE International Project Office. Report N°55/90. Wormley, England, 36 pp.

Hogg, N. G., P. E. Biscaye, W. Gardner and W. J. Schmitz, Jr. 1982. On the transport and modification of Antarctic Bottom Water in the Vema Channel. J. Mar. Res., *40* (Suppl.), 231–263.

Johns, W. E., D. M. Fratantoni and R. J. Zantopp. 1993. Deep western boundary current variability off northeastern Brazil. Deep-Sea Res., *40,* 293–310.

MacCready, P. and P. Rhines. 1993. Slippery bottom layers on a slope. J. Phys. Oceanogr., *23,* 5–22.

McCartney, M. S. 1993. Crossing of the equator by the deep western boundary current in the western Atlantic Ocean. J. Phys. Oceanogr., *23,* 1953–1974.

—— 1994. The transport of Antarctic bottom water at 4N in the western basin of the North Atlantic Ocean. J. Geophys. Res. (in press).

McCartney, M. S. and R. A. Curry. 1993. Trans-equatorial flow of Antarctic bottom water in the western Atlantic Ocean. J. Phys. Oceanogr., *23,* 1264–1276.

McDougall, T. J. and J. R. Taylor. 1984. Flux measurements across a finger interface at low values of the stability ratio. J. Mar. Res., *42,* 1–14.

McDougall, T. J. and J. A. Whitehead. 1984. Estimates of the relative roles of diapycnal, isopycnal and double-diffusive mixing in Antarctic bottom water in the North Atlantic. J. Geophys. Res., *89,* 10479–10483.

Molinari, R. L., R. A. Fine and E. Johns. 1992. The deep western boundary current in the tropical North Atlantic Ocean. Deep-Sea Res., *39,* 1967–1984.

Peggion, G. and G. L. Weatherly. 1991. On the interaction of the bottom boundary layer with deep rings. Mar. Geol., *99,* 329–342.

Pickart, R. S. and W. M. Smethie, Jr. 1993. How does the Deep Western Boundary Current cross the Gulf Stream? J. Phys. Oceanogr., *23,* 2602–2616.

Ponte, R. M., J. Luyten and P. L. Richardson. 1990. Equatorial deep jets in the Atlantic Ocean. Deep-Sea Res., *37,* 711–713.

Reid, J. L. 1989. On the total geostrophic circulation of the south Atlantic Ocean: flow patterns, tracers, and transports. Prog. Oceanogr., *23,* 149–244.

Reid, J. L., W. D. Nowlin, Jr. and W. C. Patzert. 1977. On the characteristics and circulation of the southwestern Atlantic Ocean. J. Phys. Oceanogr., *7,* 62–91.

Rhines, P. B. 1991. ATLAST a world-ocean atlas of nutrients and chemical tracers, Technical Report 91-1, School of Oceanography, Univ. of Washington, Seattle, WA, 41 pp.

Schmitt, R. W. 1979. Flux measurements on salt fingers at an interface. J. Mar. Res., *37,* 419–436.

Speer, K. G. and M. S. McCartney. 1991. Tracing lower North Atlantic deep water across the equator. J. Geophys. Res., *96,* 20443–20448.

Speer, K. G. and W. Zenk. 1993. The flow of Antarctic bottom water into the Brazil Basin. J. Phys. Oceanogr., *23,* 2667–2682.

Stommel, H. and A. B. Arons. 1960. On the abyssal circulation of the world ocean—II. An idealized model of the circulation pattern and amplitude in oceanic basins. Deep-Sea Res., *6,* 217–237.

Trowbridge, J. H. and S. J. Lentz. 1991. Asymmetric behavior of an oceanic boundary layer above a sloping bottom. J. Phys. Oceanogr., *21,* 1171–1185.

Tsuchiya, M., L. D. Talley and M. S. McCartney. 1992. An eastern Atlantic section from Iceland southward across the equator. Deep-Sea Res., *39,* 1885–1917.

—— 1994. Water-mass distribution in the western South Atlantic. J. Mar. Res., *52,* 55–81.

Warren, B. A. and K. G. Speer. 1991. Deep circulation of the eastern south Atlantic Ocean. Deep-Sea Res., *38* (Suppl.), 281–322.

Weatherly, G. L. and P. J. Martin. 1978. On the structure and dynamics of the oceanic bottom boundary layer. J. Phys. Oceanogr., *8,* 557–570.

Weiss, R. F., M. J. Warner, K. G., Harrison and W. M. Smethie, Jr. 1989. Deep equatorial Atlantic chlorofluorocarbon distributions. EOS, *70,* 1132.

Whitehead, J. A. and L. V. Worthington. 1982. The flux and mixing rates of Antarctic Bottom Water within the North Atlantic. J. Geophys. Res., *87,* 7903–7924.

Wright, W. R. 1970. Northward transport of Antarctic Bottom Water in the western Atlantic Ocean. Deep-Sea Res., *17,* 367–371.

Wüst, G. 1935. The stratosphere of the Atlantic Ocean. Scientific results of the German Atlantic expedition of the research vessel "Meteor" 1925–27; Vol. VI, section 1. English translation edited by W. E. Emery 1978, Amerind Publishing Co. Pvt., New-Delhi, 112 pp.

Zhang, H. and N. G. Hogg. 1992. Circulation and water mass balance in the Brazil Basin. J. Mar. Res., *50,* 385–420.

Received: *2 June, 1993;* revised: *22 March, 1994.*